BACHELOR'S THESIS / BIOMEDICAL ENGINEERING 2021

Cutibacterium acnes - derived extracellular vesicles: characterization and modulation of the skin immune response

MARIA POL CROS

upf. Universitat Pompeu Fabra Barcelona

Cutibacterium acnes-derived extracellular vesicles: characterization and modulation of the skin immune response

Maria Pol Cros

Bachelor's Thesis UPF 2020/2021

Thesis Supervisor(s):

Dra. María José Fábrega Fernández , (DCEXS-UPF)

Universitat Pompeu Fabra Barcelona

Acknowledgments

To begin with, I would like to emphasize that I could not have achieved my current level of success without a strong support group.

First and foremost, I would like to thank the Principal Investigator (PI) of the group, Marc Güell, for giving me the opportunity to join the Synthetic Biology group. Without him this experience would not have been possible.

I would like to express my sincere gratitude to my direct supervisor, the post-doctoral researcher María José Fábrega, for her unwavering support. Thanks to her I have acquired a lot of knowledge both theoretical and practical. When I joined the group, I did not have much experimental practice in the laboratory and with her endless patience and knowledge she has taught me how to work correctly in the laboratory and has given me the confidence to feel competent in this field. I certainly appreciate her very much since I have evolved a lot through this experience. Research is hard and often demotivating so I consider that having someone by your side who encourages you and trusts you is extremely important. I do believe that we have developed a strong bond which I would like to maintain.

I also want to thank Lorena Toloza, the microbiologist specialist in the laboratory, for making my work much more enjoyable and her help has been crucial at many times.

Moreover, I would like to show my gratitude to Júlia Mir, one of the bioinformatic scientists of the group. With her infinite knowledge of technology, she has taught me how to perform bioinformatic analysis after RNA sequencing.

I would also like to extend my gratitude to each member of the Synthetic Biology group for welcoming me so warmly and making the adaptation process in the laboratory so easy. Guadalupe has been our CRG/UPF contact throughout the process and I want to thank her too for the help she has provided with the data analysis of the extracellular vesicle samples. The proteomics analyses were performed in the CRG/UPF Proteomics Unit which is part of the Proteored, PRB3 and is supported by grant PT17/0019, of the PE I+D+i 2013-2016, funded by ISCIII and ERDF.

Last but not least, I want to thank my family, my friends and Sergi, my partner, for always being by my side and supporting me with love and understanding.

Summary/Abstract

The human microbiome plays an essential role in maintaining the host health. One of the most common bacteria present in the skin microbiota is *Cutibacterium acnes* (*C. acnes*) which is known for being involved in the homeostasis of the skin, but in some other cases, it can act as an opportunistic pathogen contributing to some skin alterations like acne vulgaris. Recently, some authors have claimed that different strains of *C. acnes* have different degrees of association with acne vulgaris. For instance, it has been shown that *C. acnes* subtype H1 was present in patients who had never developed acne vulgaris before. Therefore, a protective role has been hypothesized for this phylotype. In addition, *C. acnes* extracellular vesicles (EVs) have been reported to play an important role in the inflammatory profile of skin cells. Nevertheless, their protein, lipid and nucleic acid content have not been fully characterized yet. In the present project, EVs have been isolated from different *C. acnes* strains (A1, H1 and KPA) and their cytotoxicity has been tested with an immortalized keratinocyte cell line (HaCaT) and an immortalized sebocytes cell line (SZ95). In parallel, the immuno-modulation role of these EVs has been studied using a 2D skin inflammatory model, which mimics the *in vivo* skin layers considering both the epithelial and the immune system.

On the other hand, it is important to know the content of the EVs to determine if they could have a probiotic behavior themselves or, otherwise, be an appropriate drug delivery vehicle. RNA sequencing and a proteomic analysis are going to be conducted in order to elucidate it.

Keywords

Microbiome, Extracellular vesicles (EV), *Cutibacterium acnes*, Skin inflammation and Acne vulgaris.

Prologue

The subject for this bachelor thesis, originally stemmed from my interest in skin disorders and it has been carried out in the Department of Experimental and Health Sciences (DCEXS) of Pompeu Fabra University (UPF), particularly in the Translational Synthetic Biology group coordinated by Marc Güell Cargol. This work has been developed with the support of a María de Maeztu PostDoctoral DCEXS national grant focused on the study of *C. acnes* EVs. Moreover, at an international scale, the research group was awarded with a project to study *C. acnes* engineering funded by the Office of Naval Research-US NAVY (ONR - Science and Technology).

Index

List of Figures

List of Tables

1 Introduction

The human microbiome plays an essential role in maintaining the host health. It mainly resides on the skin, on the oral mucosa, and in the gastrointestinal tracts, and has fundamental roles in health and disease [1]. The skin is the human body's largest organ and it consists of three layers - the epidermis, the dermis and the subcutaneous fat layer (hypodermis)- which have different and specific functions. The epidermis is the outer layer of the skin, defined as a stratified squamous epithelium, primarily comprising of keratinocytes in progressive stages of differentiation. The prime function of the epidermis is to act as a physical barrier, protecting our bodies from the invasion of foreign pathogens or toxic substances. At the same time, it prevents the loss of water and maintains internal homeostasis. The dermis forms the inner layer of the skin and it contains blood and lymph vessels, nerves and other structures, such as hair follicles and sweat glands. Its main function is to sustain and support the epidermis but it also plays an important role in wound healing. The hypodermis is the subcutaneous layer lying below the dermis; it consists largely of fat and provides the main structural support for the skin as well as insulating the body from cold and aiding shock absorption. It is interlaced with blood vessels and nerves [2].

The skin is colonized by a diverse collection of microorganisms – including bacteria, viruses, fungi and archaea – most of which are harmless or even beneficial to their host [3]. These microbial communities grow and diversify until puberty, when hormonal and developmental changes help to sculpt the final composition that is carried into adulthood. Over the past decade, researchers have uncovered evidence of extensive communication between bacteria, skin cells and immune cells. These interactions are aimed at reinforcing and repairing the barrier formed by the skin, bolstering the body defenses against infection and tamping down excess inflammation [4]. Nevertheless, failure of this communication can break down the protective barrier of the skin and cause a dysbiosis between commensals and pathogens which, in turn, can lead to the development of systemic diseases [5].

Nevertheless, the diversity of the human microbiota at the strain level and its association with human health and disease is largely unknown. Many studies have shown that microbe-related human diseases are often caused by certain strains, rather than the entire species being pathogenic [6]. These distinct phylogroups vary with respect to a wide range of characteristics, including cellular morphology, inflammatory and immunogenic properties, production of virulence factors among others, which may help to explain the differences in their associations with health and disease [7].

One of the most common bacteria present in the skin microbiota is the Gram-positive anaerobic bacterium, *Cutibacterium acnes* (*C. acnes*) which dominates pilosebaceous units [7]; complex mini-organs of the body that display considerable morphological, microbiological and metabolic diversity depending on the location of the skin [8].

C. acnes is known to be involved in the homeostasis of the skin but in some other cases, given the correct set of conditions (Fig. 1), it can act as an opportunistic pathogen involved in some skin alterations such as acne vulgaris, eczema and psoriasis. Remarkably, dermatological diseases are the 4^{th} leading cause of non-fatal diseases worldwide. Skin conditions pose a significant threat to patients' well-being and their ability to be involved and engaged in relationships with others [9].

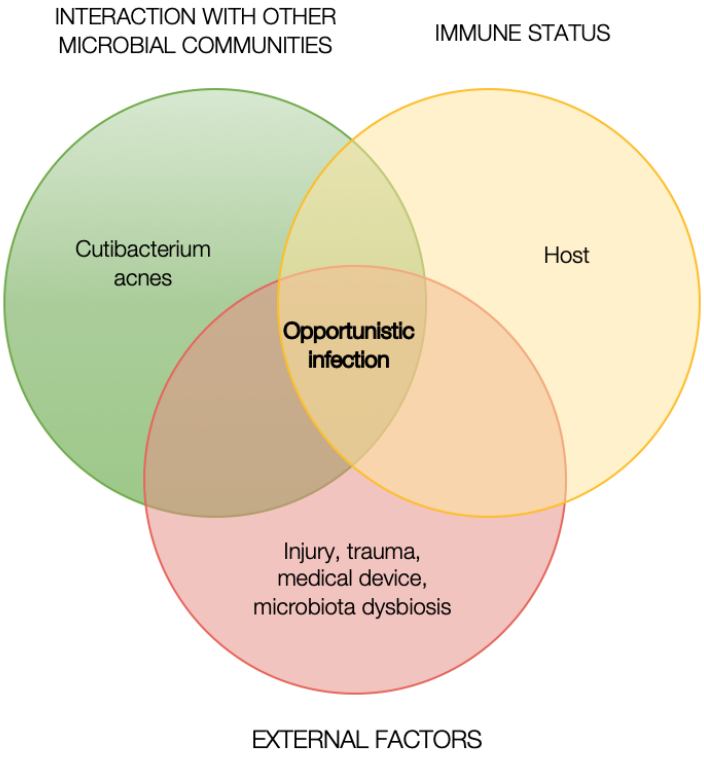

Figure 1: Factors that could trigger an opportunistic infection caused by *C. acnes*.

Acne vulgaris, commonly known as acne, is one of the most common skin diseases, with an 85% rate of prevalence in those aged 12-24 years [10]. It is considered a disease of the pilosebaceous unit. The sebaceous gland, in particular, actively responds to hormonal, environmental and immunological fluctuations. The development of acne is not only specific to an individual but also to the location, with only some follicles developing inflammation even during severe manifestations of the disease [7]. The burden of this condition in an adolescent's life is recognized through studies which reveal anxiety in social interaction, dissatisfaction with appearance, reduced self-esteem and overall impaired quality of life [9, 11, 12]. Therefore, the knowledge of the psycho-social problems related to acne is important in determining optimal healthcare.

Although the etiology and pathogenesis of acne is not clear yet, microbiome alterations are considered to be one of the main mechanisms contributing to the development of acne [1]. Recently, some authors have explained that different strains of *C. acnes* have different degrees of association with acne vulgaris [6, 7, 13]. For instance, it has been shown that *C. acnes* subtype H1 was present in patients who had never developed acne vulgaris before [1]. Therefore, a protective role has been hypothesized for this phylotype. On the other hand, *C. acnes* subtype A1 was significantly associated with acne [8]. The commensal bacterial strain KPA is also analyzed in the present project, nonetheless, little information on this phylotype is found in previous scientific publications.

The interest of the project lies in determining what role the vesicles secreted by *C. acnes* play in the development of acne. However, why is there so much interest in the study of vesicles in the scientific community? Extracellular vesicles (EVs) have been reported to conduct critical pathophysiological functions as a mode of communication in bacteria [14]. Bacteria secrete diverse factors to communicate with or evoke cellular responses from target cells.

Like mammalian cells, most Gram-negative and Gram-positive bacteria release EVs too. EVs are nano-sized lipid bilayer vesicles constantly secreted by most cells, including archaea, bacteria and eukaryotic cells, into the extracellular environment [15]. One of the most intriguing questions that has prompted a great deal of research within recent years is "what do bacterial EVs carry inside them?" As a matter of fact, they have been considered to be cargo structures that harbor different molecules of significant relevance for the interaction with the host, both in negative and positive ways [16]. They contain specific subsets of proteins, DNA, RNA and lipids that represent their cellular status. Moreover, EVs are also involved in immune modulation, angiogenesis and transformation of cells by transferring proteins, lipids and nucleic acids from a cell of origin to recipient cells [17, 18].

The recent technical advances in proteomics have accelerated the characterization of EVs, revealing that their cargo reflect the cellular changes that occur in physiological and pathological conditions [19]. A proteomic characterization of *C. acnes* EVs may reveal new proteins and molecular networks that affect the normal physiology of the skin microbiota and may lead to the development of acne. Moreover, it will allow the identification of biomarker candidates that are unique to each strain of EVs.

On the other hand, several mechanisms of cell-cell communication have now been proven to exist, such as chemical receptor-mediated events, direct cell-cell contact and cell-cell synapses. Valadi et al. (2007) [20] suggested a new mechanism of cell-cell communication which was the delivery of small RNAs by transfer through EVs, increasing the complexity by which cells can communicate. It is very likely that this genetic communication takes place in a micro-environment, but it could also occur at a distance, by trafficking of EVs through the systemic circulation in a hormone-like manner. Moreover, they detected the presence of small RNAs in EVs which suggested that EVs may contain miRNAs. Subsequently, numerous articles have been published studying miRNAs encapsulated in EVs, which have been considered as candidate interspecies-communication molecules, due to their demonstrated capacity to modulate gene expression in multiple cell types and species [21].

Initially, EVs were considered cargo structures transporting information from secretory to receptor cells, but nowadays new insights have verified that they play a pivotal role in inter-kingdom communication and immune modulation. For instance, in 2020 Bajic et al. observed differential effects of EVs derived from different Gram-positive bacteria in terms of inflammatory cytokine induction [16]. Therefore, the analysis of EVs molecular cargo including only protein and RNA components in *C. acnes* is essential to understand which information they contain and which signaling pathways they modulate in the host cell, to determine the differences between the distinct *C. acnes* phylotypes and to have a more tangible idea of the therapeutic potential of EVs.

1.1 Objectives

In the present project, the main objective is focused on determining whether the effect attributed to the different *C. acnes* strains in terms of pathogenicity and involvement in the development of acne is due to the EVs secreted by them. In more detail, the specific objectives are:

1. To establish a proper protocol to isolate *C. acnes* EVs from three different strains (A1, H1 and KPA).
2. To visualize EVs under microscopy and to determine their shape and size.
3. To describe the miRNAs profile encapsulated within *C. acnes* EVs by RNA sequencing analysis.
4. To characterize *C. acnes* EVs in terms of protein content by proteomic analysis.
5. To perform *in vitro* cytotoxicity assays in human cell lines of the skin to determine whether EVs affect host cell viability.
6. To develop *in vitro* models mimicking healthy and inflamed skin to test *C. acnes* EVs potential.

2 Methods

2.1 Bacterial conditions of *C. acnes* cultures

The *C. acnes* strains used were A1, H1 and KPA, all of them donated by the company S-Biomedic. Initial cultures were always started from glycerol stocks (stored at −80°C) and seeded in Brucella agar plates which were incubated from 4 to 5 days at 37°C in anaerobic conditions using the BD GasPak™ EZ Anaerobe pouch System.

2.2 Isolation process of EVs

The method used for EVs isolation is comprised of several steps: cultivation, centrifugation, concentration or ultrafiltration and ultracentrifugation (Fig. 2).

In the cultivation step, *C. acnes* strains A1, H1 and KPA were collected from a Brucella agar plate using sterile swabs (Deltalab) and were transferred into 1 L of Brucella liquid medium. After 7 to 10 days at 37°C with 600 rpm of stirring and maintaining anaerobic conditions, the culture was centrifuged in sterile 250 mL bottles at 10000 x g for 30 minutes and at 4°C. For this step, a Beckman Coulter Avanti JXN-26 high velocity centrifuge with the J-LITE JLA-16.250 Fixed-Angle Aluminum Rotor was used. Then, the pellet was discarded, and the supernatant (SN) was filtered using the Thermo Scientific™ Nalegene™ Rapid-Flow™ 75 mm Filter Unit (500 mL) to avoid bacterial contamination. Subsequently, it was concentrated by a Centricon Plus-70 10 KDa system using the JS-5.3 Swinging-Bucket Rotor. To ensure free contamination during the process, an extra step of 0.22 μm filtration was added into the protocol. The filtrated and concentrated SN, was then ultra-centrifuged using the JA-25.50 Fixed-Angle Rotor at 75600 x g for 3 hours and at 10°C to precipitate the EVs. The pellet containing the isolated *C. acnes* EVs was washed with 1X PBS and ultra-centrifuged again for 1 hour keeping the same conditions as in the previous step. Finally, the SN was discarded, and the pellet obtained was resuspended with 200 μL of PBS buffer and kept in an Eppendorf at −20°C. To ensure non-bacterial presence in EVs samples, 10 μL of each batch were seeded in a Brucella agar plate and incubated from 4 to 5 days at 37°C in anaerobic conditions.

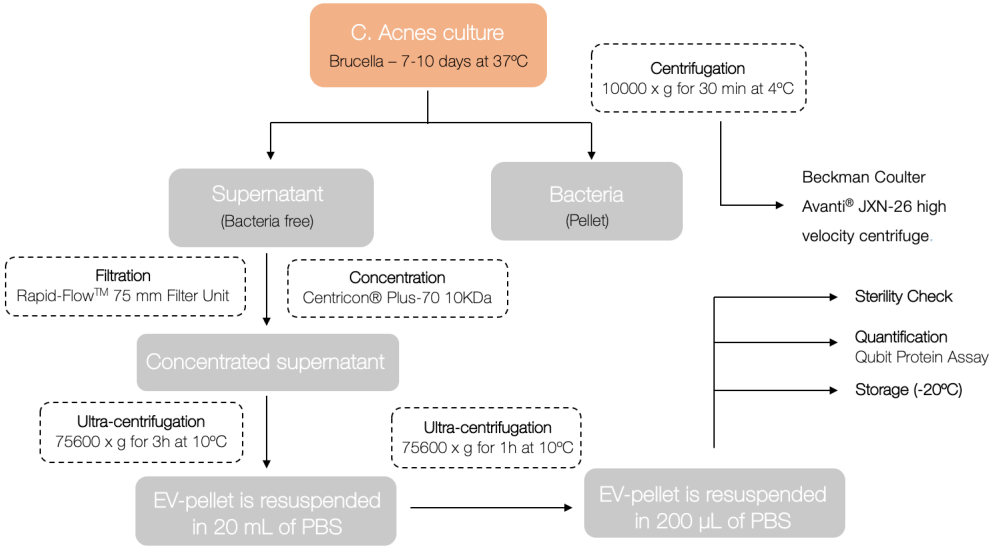

Figure 2: Schematic representation of the EVs isolation process.

2.3 Qubit protein assay

The Qubit Protein Assay Kit (Thermo Fisher Scientific) has made protein quantification of the EVs easy and accurate. The kit includes concentrated assay reagent, dilution buffer and three different prediluted BSA standards. The first step in this process is to prepare the Qubit working solution by diluting the Qubit Protein Reagent 1:200 in Qubit Protein Buffer. Each standard tube is prepared adding exactly 10 μL of each Qubit standard to 190 μL of the Qubit working solution. The quantity of sample to be analyzed can be anywhere from 1–20 μL. Then, the corresponding volume of Qubit working solution is added to each assay tube: anywhere from 180–199 μL. Careful pipetting in this assay is important in order to avoid the creation of bubbles since it could affect the results. Afterwards, the concentration of protein (mg/mL) of the EVs was read using the Qubit Fluorometer (Thermo Fisher Scientific).

This assay was performed at room temperature using specific Qubit assay tubes (Cat. no. Q32856).

2.4 Negative staining and Transmission Electron Microscopy

Isolated *C. acnes* H1 EVs were examined by Transmission Electron Microscopy (TEM) after negative staining as described in previous publications [22]. In this specific case, EVs were resuspended with TRIS buffer since PBS is not compatible with uranyl acetate. A drop of EVs suspension was absorbed for 2 minutes on Formvar/carbon coated-grids that were previously activated by UV light. The grids were washed with distilled water, stained with 2% uranyl acetate for 1 minute, air dried and examined by TEM (Parc Científic de Barcelona). Fig. 3 illustrates the configuration used to perform the negative staining.

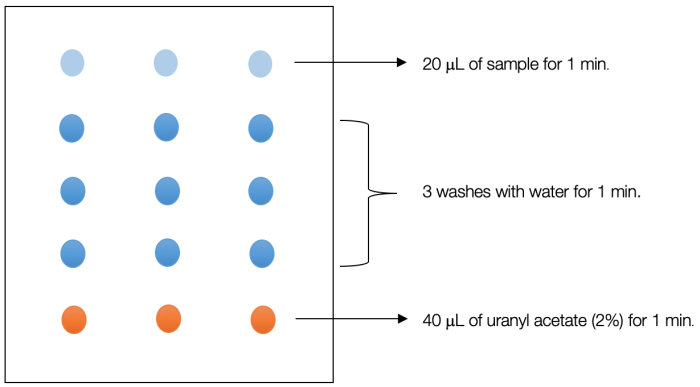

Figure 3: Standard configuration for negative staining with 2% uranyl acetate.

2.5 Nanoparticle Tracking Analysis (NTA) of EVs

EVs resuspended with 200 μL of PBS were sent to *Institut de Ciència de materials de Barcelona* in order to be analyzed with the Malvern Nanosight NS300 instrument. This system uses Nanoparticle Tracking Analysis (NTA) technology as to detect and visualize populations of nanoparticles. These EVs are visualized by light scattering using a light microscope (Fig. 4). A video is taken and the NTA software tracks the Brownian motion of individual EVs and calculates their size and total concentration.

One of the main advantages of this quantification method is that the flow mode used allows a large number of particles to be measured in a small time-frame, resulting in more accurate measurements with less variance [23].

In order to analyze properly the samples sent, triplicates were made by *Institut de Ciència de materials de Barcelona*. Mean size (nm), mode size (nm), and concentration (particles/mL) were obtained, and high-resolution particle size distribution profiles and concentration measurements were provided.

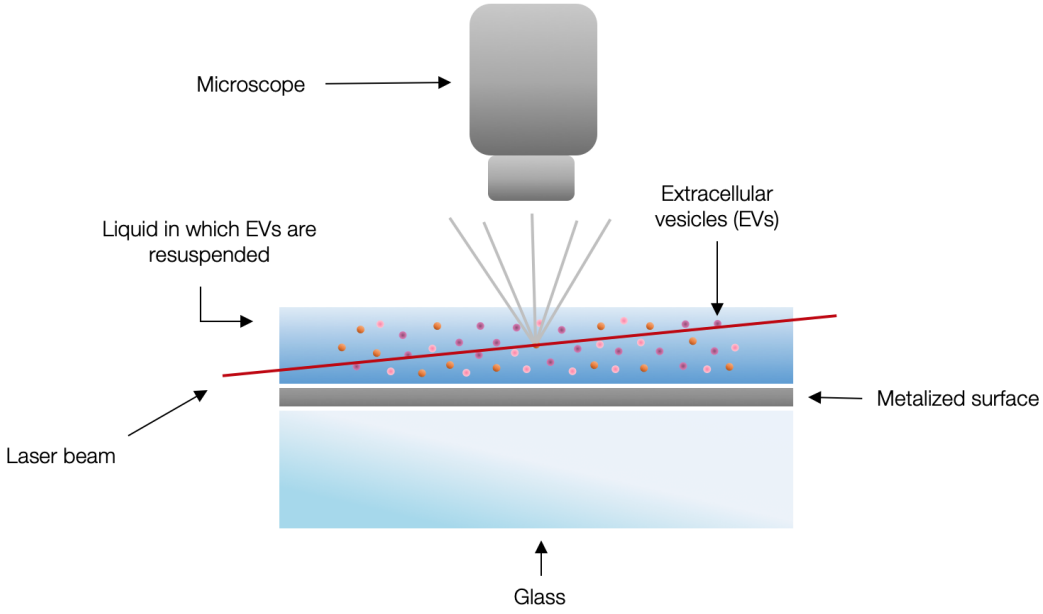

Figure 4: Nanosight NS300 instrument configuration.

2.6 Isolation of EVs RNA and sequencing analysis

Three independent batches of A1 and H1 EVs were necessary to obtain enough RNA quantity for its subsequent analysis. The RNA was extracted using the miRNesay Mini Kit (Qiagen) following the manufacturer's protocol. Quality and RNA concentration were checked by the absorbance ratio at 260 and 280 nm in a Thermo Scientific™ NanoDrop™ One^C Spectrophotometer. RNA samples were sent to Macrogen for library preparation and RNA sequencing.

The general workflow for Next Generation Sequencing (NGS) (Fig. 5) is divided into four main processes: dedicated sample preparation, library preparation, sequencing itself and bioinformatics analysis [23].

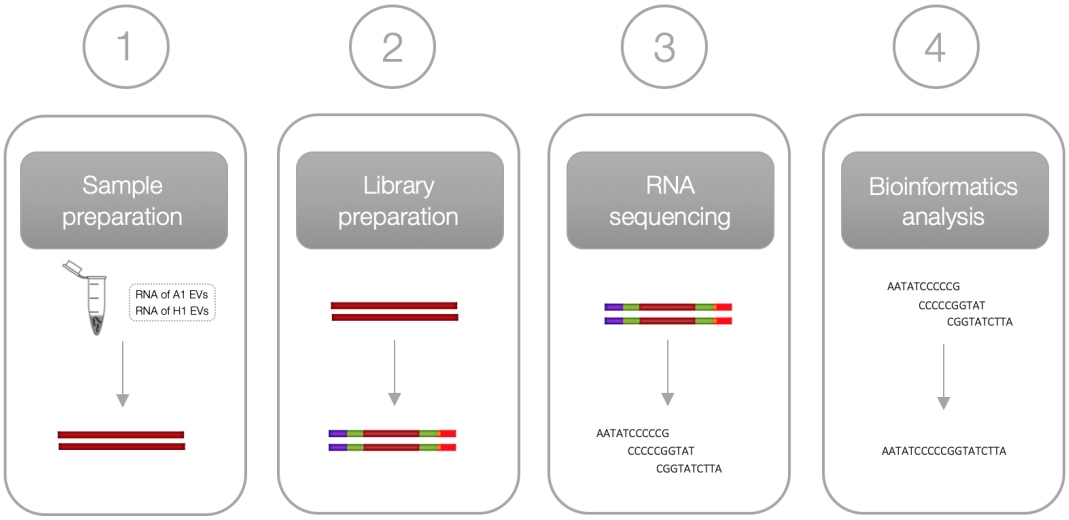

Figure 5: **General workflow for NGS.** First of all, the RNA sample has to be extracted from the EVs sample, in this case, from A1 and H1 *C. acnes* EVs. Library preparation consists of converting the RNA to cDNA of defined lengths with oligomer adapters at the 5' and 3' ends to be compatible with the sequencing technique to be used. Then, the sequencing itself takes place on the respective system. Finally, the generated data is analyzed using bioinformatics to obtain meaningful data.

By doing background research [24, 25], the miRNA size selected for the library preparation was from 15 to 200 base pairs (bp). Macrogen used the Library prep Kit, SMARTer smRNA-Seq Kit for Illumina (Cat. Nos. 635029, 635030, 635031) which is designed to generate high-quality RNA libraries for sequencing on Illumina platforms. This kit enables users to analyze diverse RNA species, including miRNA, piRNA, snoRNA and snRNA, from inputs of total RNA or enriched smRNA.

The resulting sequencing data was sent to us for bioinformatics analysis. The pipeline followed to do so was described by Potla et al. (2021) [26] and some changes were included. Briefly, the pipeline consists of several steps: quality control, trimming and mapping against the reference genome.

Before starting analyzing any data, the number of reads for each *C. acnes* strain (A1 and H1) were counted. Then, it was necessary to ensure the reads were of sufficient quality for subsequent analyses. For this, quality control was performed to avoid poor quality input since this will result in poor quality data. The quality of raw sequencing reads was checked using a metric called Q score or Phred quality score, which serves as a compact way to communicate very small error probabilities. A Q score of 30 (99.9% of accuracy) is considered accepted in the bioinformatics field. Afterwards, it is important to remove the low-quality portions of the raw reads while preserving the longest high-quality part of a read. This pre-alignment procedure is called read trimming and it is crucial for efficient mapping. The trimming was done following the recommendations of Illumina's Library Prep Kit and the tool used was Cudadapt[1]. Since miRNA sequencing produces very short reads, accurate alignment requires strict parameters to avoid multiple matches in the reference database.

[1]Cutadapt - Software: Adapter Trimming - https://cutadapt.readthedocs.io/en/stable/

In this case, the alignment of reads was perfomed to the human database from miRBase[2] using the original version of Bowtie [3]. The alignment was done against the database of mature human miRNA sequences and also against the database of hairpin human miRNA sequences. The reads that were not aligned to miRBase were then aligned to the genomic coordinates of the mature miRNA from the Human Reference Genome. These aligned reads have been sorted and filtered using Samtools[4].

Finally, only those regions which fell within the coordinates provided by miRbase were annotated giving a final count for the known miRNAs found in each sample.

2.7 Purification of EVs total protein: Proteomic analysis

In order to determine the composition of its proteome, EVs were lysed with the Freezer Mill and precipitated using a protocol provided directly by the proteomics service.

When isolated, EVs were kept in 200-300 μL of PBS. Subsequently, 20-30 μL of RIPA 10X buffer (Merk Millipore) and cOmplete™ Protease Inhibitor tablets (Roche) were added. Specifically, 1 mL of RIPA 10X buffer was used and mixed with 1 tablet. Liquid nitrogen (N_2) was used to obtain beads of the pellet of each *C. acnes* strain to be introduced in the Freezer Mill, a small cryogenic mill. Only 0.5 g of beads could be introduced into the Freezer Mill in order to properly lyse the EVs. The Freezer Mill conditions established were: precooling for 5 minutes, running step for 2 minutes, 2 cycles of interval and at a rate of 10 cycles per second (CPS). After introducing the samples into the Freezer Mill, a powder was obtained and it was resuspended with the solution of RIPA buffer and cOmplete™ Protease Inhibitor tablets prepared previously. Afterwards, precipitation with acetone was performed following the protocol provided directly by the proteomics service. It had to be considered that 8 μg was the minimum quantity accepted for the proteomic analysis. Finally, the precipitate was resuspended with an amount ranging from 50 μL to 250 μL of 6M Urea.

Qubit protein assay was performed to assess the approximate quantity of protein in each sample.

After preparation, the lysed samples were analyzed by the UPF/CRG Proteomics Unit. The protocol used is provided in section 7.1.1 of Supplementary information.

2.8 *In vitro* testing

2.8.1 Human cell lines

The biological niche in which *C. acnes* EVs act comprises keratinocytes, sebocytes and lymphocytes. The immortalized lines used for these cell types were HaCaT, SZ95 and Jurkat respectively.

The immortalized keratinocytes cell line (HaCaT), bought in the American Type Culture Collection (ATCC), was cultured in T-75 culture flasks (Thermo Scientific) with Dulbecco's Modified Eagle Medium (DMEM, Gibco) supplemented with 10% of Fetal Bovine Serum (FBS) and 0,1% of penicillin and streptomycin. They were incubated at 37°C in 5% of CO_2, 95% of humidity until 90-100% of confluency.

[2]miRBase - Database: mature and hairpin miRNA sequences - http://www.mirbase.org/

[3]Bowtie1 - Software: Read alignment - http://bowtie-bio.sourceforge.net/index.shtml

[4]Samtools - Software: Processing aligned files - http://www.htslib.org

The immortalized sebocytes cell line (SZ95) was donated by the Laboratory for Biogerontology, Dermato-Pharmacology and Dermato-Endocrinology at the Departments of Dermatology, Venereology, Allergology and Immunology of the Dessau Medical Center. Sebocytes were cultured in T-75 culture flasks (Thermo Scientific) with Sebomed basal medium (DMEM/F12, Gibco) supplemented with 10% of Fetal Bovine Serum (FBS), 0,1% of penicillin and streptomycin, 5 ng/mL of recombinant human Epidermal Growth Factor (EGFr) and 500 μL of filtrated $CaCl_2$ 1M. They were incubated at 37°C in 5% of CO_2, 95% of humidity until 90-100% of confluency.

The immortalized T lymphocytes cell line (Jurkat, Clone E6-1), bought in the American Type Culture Collection (ATCC), was cultured in T-75 culture flasks (Thermo Scientific) with Roswell Park Memorial Institute medium (RPMI, Gibco) supplemented with 10% of Fetal Bovine Serum (FBS) and 0,1% of penicillin and streptomycin. They were incubated at 37°C in 5% of CO_2, 95% of humidity until 90-100% of confluency.

2.8.2 Cytotoxicity assay

At that point, $2 * 10^5$ cells/mL were seeded in two different 96-well plates. After 24 hours had passed, HaCaT cells and SZ95 cells were incubated with 1000 μg/mL, 500 μg/mL ,250 μg/mL , 125 μg/mL, 50 μg/mL, 25 μg/mL, 12.5 μg/mL, 6.25 μg/mL, 3.125 μg/mL, 1.56 μg/mL, 0.78 μg/mL, 0.39 μg/mL and 0.195 μg/mL of H1 *C. acnes* EVs for 24 hours at 37°C in 5% of CO_2 and 95% of humidity.

To evaluate cytotoxicity, an MTT assay was performed. This colorimetric assay is based on the reduction of a yellow tetrazolium salt (MTT) to purple formazan crystals by cells which are metabolically active. These viable cells contain mitochondrial dehydrogenases which reduce MTT to formazan. Therefore, MTT reagent (Thermo Fisher Scientific) was added to each well and incubated for, approximately, 3 hours. Then, in order to quantify it, cells were incubated with the organic solvent dimethyl sulfoxide (DMSO) for 10 minutes in order to lyse the cells and dissolve the formazan crystals. The darker the solution, the greater the number of viable, metabolically active cells. Their absorbance was measured at 595 nm using the plate reader (Tecan). Afterwards, the percentage of viability of target cells was calculated as follows:

$$\% \text{ Cell viability} = \frac{\text{Mean absorbance in test well}}{\text{Mean absorbance of control well}} * 100 \quad (1)$$

2.8.3 *C. acnes* EVs treatment

Different *C. acnes* EVs were incubated with HaCaT, SZ95 and Jurkat immortalized cell lines. To do so, $2 * 10^5$ cells/mL were seeded in a 12-well plate for all three cell types. After 24 hours had passed, all cell types were incubated with EVs from *C. acnes* A1, H1 and KPA. All three plates were divided into three rows - one for each *C. acnes* strain - and each row had a control well and different concentrations of EVs, to be precise, 12.5 μg/mL, 25 μg/mL and 50 μg/mL.

In all cases, gene expression levels were evaluated by RT-qPCR.

2.8.4 Inflammatory model

To test the best condition for a positive control in our skin inflammation model several inflammatory reagents have been tested.

Two inflammatory reagents were selected to be tested in our *in vitro* model of HaCaT: Arachidonic acid (AA) (Sigma Aldrich), and Lipopolysaccharide (LPS) solution 500X (Invitrogen). For that, $2 * 10^5$ HaCaT/mL were seeded in a 12-well plate. The following day, different concentrations were tested depending on the chosen reagent. For the AA assay, the following concentrations were tested, 5 μM, 10 μM, 50 μM, 100 μM and 150 μM during 24 hours. For the LPS assay, the concentrations of 2.5 μg/mL, 12.5 μg/mL and 25 μg/mL were tested, after 24 hours, on the cells.

The two inflammatory reagents selected to be tested with the *in vitro* model of SZ95 were LPS and palmitic acid (PA) (Sigma Aldrich). For that, $2*10^5$ SZ95/mL were seeded in a 12-well plate. For the LPS assay, the concentrations of 1 μg/mL, 10 μg/mL and 25 μg/mL were tested, after 24 hours, on the cells. For the PA assay, the concentrations of 10 pg/mL, 50 pg/mL and 100 pg/mL were tested, after 24 hours, on the cells.

The inflammation was evaluated by RT-qPCR.

2.8.5 2D skin inflammatory model

For this experiment, a Transwell System was used to do the co-cultures. Using a 12-well plate, lymphocytes (Jurkat cells) were seeded in the basolateral compartment ($2*10^5$ cells/mL per well in a volume of 1500 µL) while keratinocytes (HaCaT cells) were cultured in the apical compartment or insert ($2 * 10^5$ cells/mL in a final volume of 500 µL). Both cell types are communicating only by secreted soluble factors, and not by direct contact.

Inflammation mediated by LPS was induced using a concentration of 12.5 μg/mL.

Gene expression levels for pro-inflammatory cytokines were evaluated by RT-qPCR.

2.8.6 Real time quantitative PCR analysis (RT-qPCR)

Total RNA was extracted from HaCaT, Sebocytes and Jurkat cells using the miRNesay Mini Kit (Qiagen) following the manufacturer's protocol. Purity and RNA concentration were measured by the absorbance ratio at 260 and 280 nm in a Thermo Scientific™ NanoDrop™ One^C Spectrophotometer.

RNA was reverse transcribed using the cDNA Reverse Transcription Kit (Thermo Fisher Scientific) in a final volume of 20 μL following the manufacturer's recommendations. The retro transcription reaction was conducted in the ProFlex PCR System (Applied Biosystems). RT-qPCR reactions were performed in QuantStudio™ 7 Flex Real-Time PCR System (Applied Biosystems) by using SYBR Green PCR Master Mix (Applied Biosystems) and specific primers for each cell type. See the list of primers in Table 2 at the section 7.1.2 of the Supplementary Information. A control reaction was performed with water in which no RNA was present. The $2^{-\Delta\Delta Ct}$ method was used to normalize expression results. The values of the housekeeping CREBBP gene were used to normalize the values obtained for each of the genes under study.

2.9 Statistical analyses

Statistical analysis was performed using GraphPad. All assays were repeated independently at least three times in triplicate. The values for all measurements are presented as the mean ± standard deviation (SD). Differences between more than two groups were assessed using one-way ANOVA followed by Dunnett's test. Data with a p value less than 0.05 were considered statistically significant.

3 Results

3.1 Negative staining and Transmission Electron Microscopy

C. acnes H1 EVs were isolated from cell-free culture supernatants and evaluated by negative stain-TEM. Images show spherical vesicles ranging in size from approximately 70–100 nm in diameter (Fig. 6).

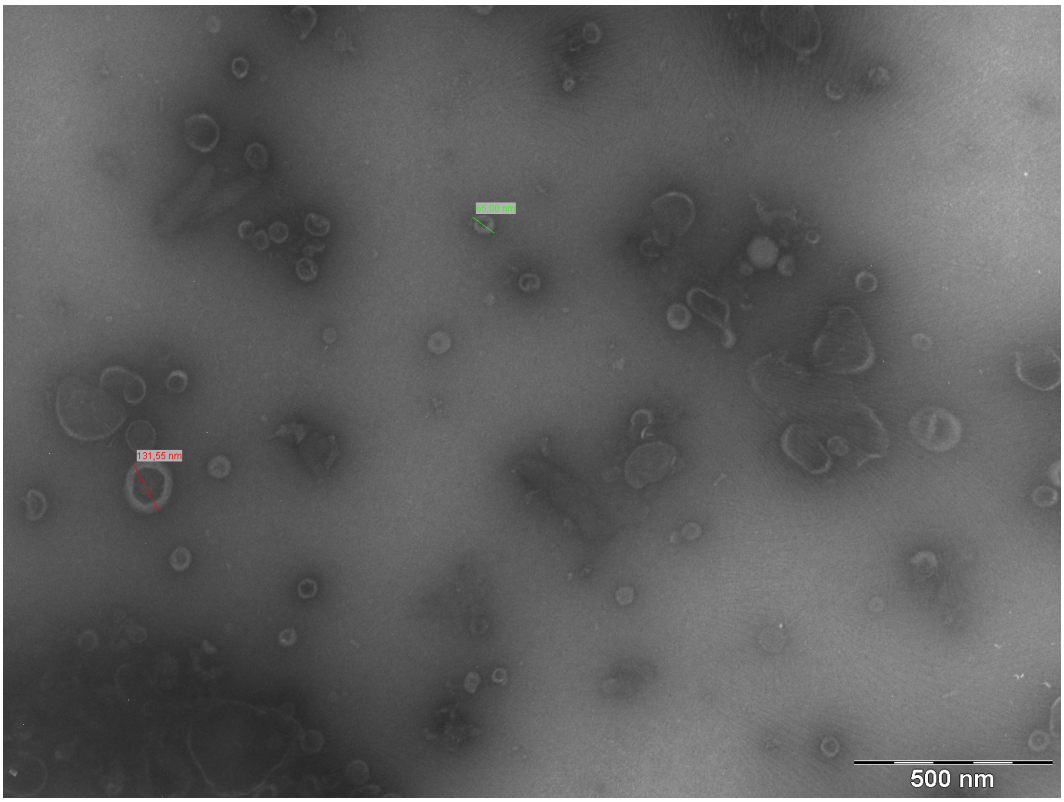

Figure 6: Negative staining electron microscopy of isolated *C.acnes* H1 EVs.

3.2 Nanoparticle Tracking Analysis (NTA) of EVs

To validate the TEM results, NTA was performed as it has provided high-resolution particle size distribution profiles and also concentration measurements.

The average of five reads was calculated and plotted as particle size versus number of particles per mL. Fig. 7 shows the size distribution graphs for each *C. acnes* strain.

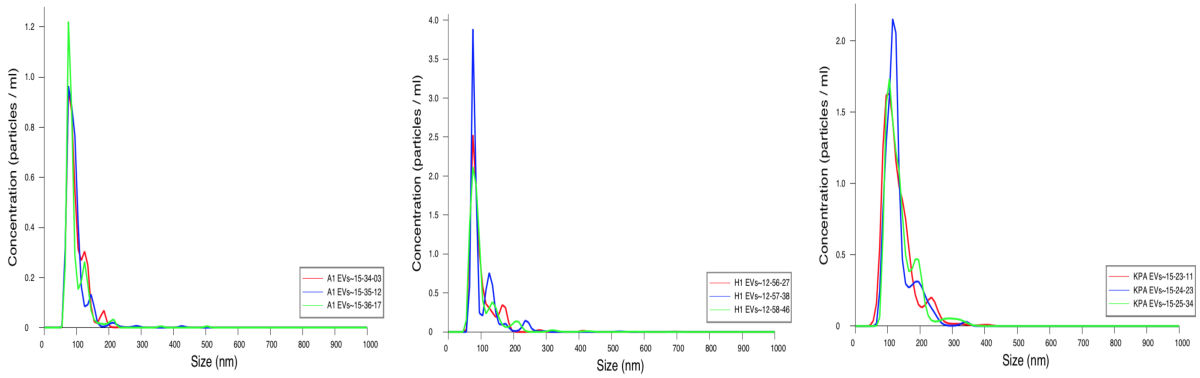

(a) A1 EVs (b) H1 EVs (c) KPA EVs

Figure 7: EVs isolated from *C. acnes* A1, H1 and KPA strains were diluted 1:5000, 1:1000 and 1:1000 respectively in PBS and measured using Nanosight NS500. All data represents the mean of three independent experiments ± standard error.

On the other side, as Fig. 8 shows there is some variation in scattering intensity between particles of the same size in triplicates of each strain, especially in KPA EVs. Values obtained after NTA show that KPA EVs are the ones that have the highest mean vesicle size. Nevertheless, in terms of concentration, A1 is the strain that has the highest yield rate of EVs' secretion ($3.92 * 10^{12}$ EVs/mL), four times more than H1 ($9.48 * 10^{11}$ EVs/mL) and three times more than KPA ($1.23 * 10^{12}$ EVs/mL) (Table 1).

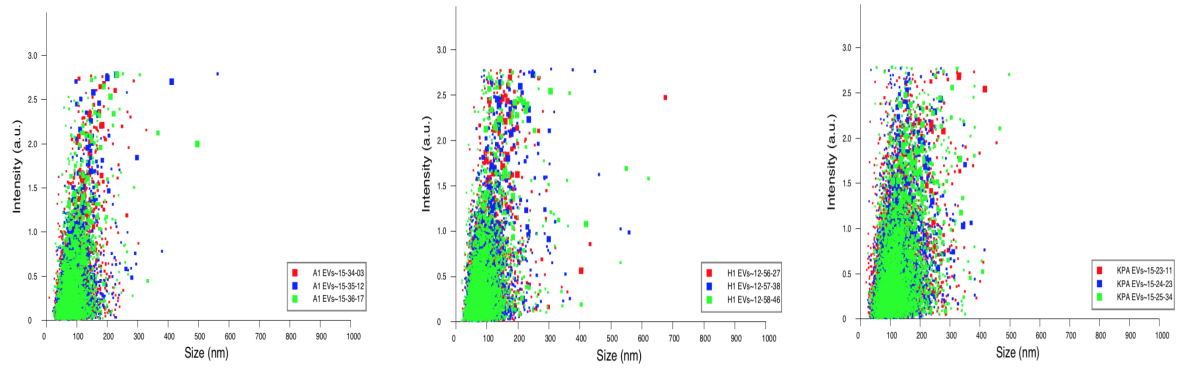

(a) A1 EVs (b) H1 EVs (c) KPA EVs

Figure 8: **EVs scattering distribution.** EVs isolated from *C. acnes* A1, H1 and KPA strains were diluted 1:5000, 1:1000 and 1:1000 respectively in PBS and measured using Nanosight NS500. All data represents the mean of three independent experiments ± standard error.

C.acnes strain	Mean ± SE (nm)	Mode ± SE (nm)	SD ± SE (nm)	Particles/mL ± SE
A1 EVs	96.8 ± 0.5	78.4 ± 0.5	33.8 ± 3.1	$3.92 * 10^{12} \pm 1.31 * 10^{11}$
H1 EVs	100.7 ± 0.7	76.8 ± 0.4	47.4 ± 2.1	$9.48 * 10^{11} \pm 1.33 * 10^{10}$
KPA EVs	133.0 ± 2.3	107.6 ± 5.5	46.2 ± 2.0	$1.23 * 10^{12} \pm 3.20 * 10^{10}$

Table 1: **Summary of NTA data.** Mean vesicle size (nm), mode size (nm) and concentration (particles/mL) ± Standard Error (SE) (nm), were evaluated for A1, H1 and KPA EVs.

In addition, recordings of the different types of *C. acnes* EVs were obtained from the NTA analysis (see Videos).

3.3 Pilot study: RNA sequencing analysis

C. acnes genome is barely characterized. Most of the small RNAs are not annotated in any database. Therefore, a first mapping with the Homo Sapiens genome has been performed. As commented earlier, during the bioinformatics analysis a pipeline has been followed. One of the most relevant steps was to ensure the reads were of sufficient quality for subsequent analyses. A quality score, named Q or Phred score, of 30 was the expected in this case. Plots verifying this quality accuracy are shown in the Supplementary Information section 7.2.1. The miRNAs found that were considered more relevant in both A1 and H1 are: hsa-miR-8485 and hsa-miR-10b-3p. The percentage of mapped reads falling into those two miRNAs are 37.37% and 12.46% in A1 EVs nucleic cargo respectively and 5.86% and 23.98% in H1 EVs.

3.4 Proteomic analysis

To characterize the protein profile of A1, H1 and KPA *C. acnes* EVs, the whole protein content was isolated and analyzed by Mass Spectrometry by the UPF/CRG Proteomics Facility.

The creation of the Venn diagram allowed a first comparative study in which the amount of proteins shared by the three different *C. acnes* strains was determined. To do so, only the high-confidence proteins that were detected in more than two replicates of the three *C. acnes* strains were selected. As Fig. 9. illustrates, the three strains share 382 proteins. This amount is considerable but not surprising since they come from a common organism. In addition, a pair comparison was conducted and the results show that A1 and H1 share 171 proteins, A1 and KPA share 66 proteins and H1 and KPA share 72 proteins. Finally, by looking at the proteins unique to each strain it is shown that, A1 is the strain which has the highest amount of high-confidence proteins identified, 396 to be precise, followed by H1 in which 100 high-confidence proteins were identified and KPA in which only 42 high-confidence proteins were identified.

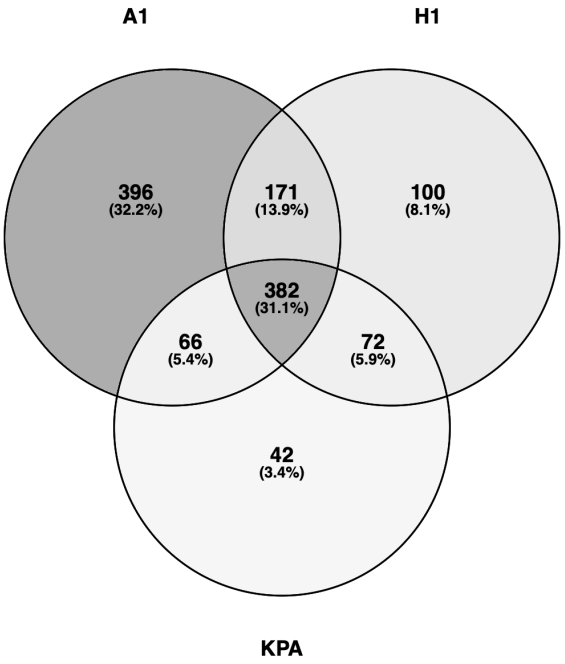

Figure 9: Venn diagram showing the relationship between A1, H1 and KPA

Using UniProt database, a Gene Ontology (GO) analysis has been carried out allowing the description of the proteins considering their molecular function, the biological processes in which they are involved and their cellular location. This first classification gives a general overview of the quantity of proteins present in each domain.

Of the cellular components, *C. acnes* A1 EVs contain 43 membrane-associated (10.91%), 40 cytoplasmic (10.15%) and 1 extracellular region (0.25%) proteins (Fig. 10.A). *C. acnes* H1 EVs contain 24 membrane-associated (24%), 12 cytoplasmic (12%) and 1 extracellular region (1%) proteins (Fig. 10.B). *C. acnes* KPA EVs contain 8 membrane-associated (19.05%), 4 cytoplasmic (9.52%) and 1 extracellular region (2.38%) proteins (Fig. 10.C).

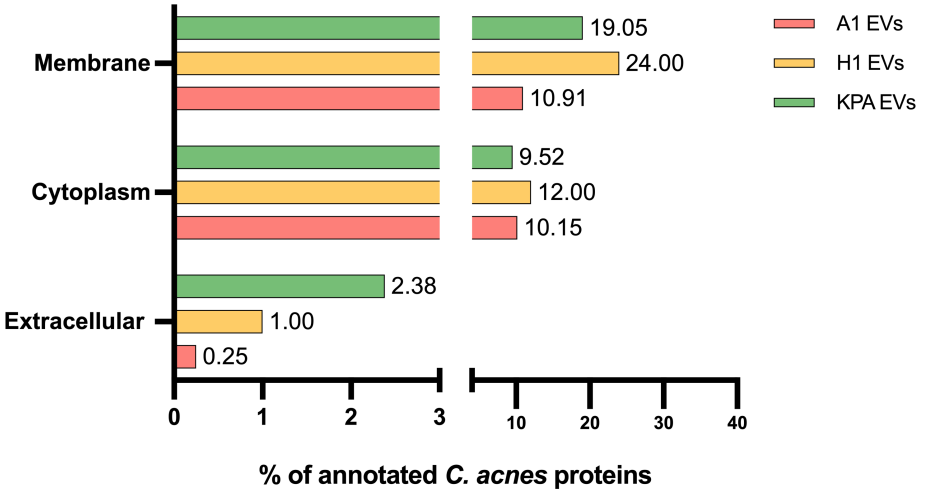

Figure 10: **Proteomic profile of *C. acnes* EVs.** Gene Ontology (GO) term of cellular components of *C. acnes* A1 EVs, *C. acnes* H1 EVs and *C. acnes* KPA EVs.

The biological processes and molecular functions of the proteins found in *C. acnes* EVs are gathered in Fig. 11. *C. acnes* A1 EVs contain 131 proteins involved in cellular processes (33.25%), 113 in metabolic processes (33.76%), 40 in quorum sensing (10.15%), 17 in localization (4.31%), 17 in biological regulation (4.31%), 8 in response to stimulus (2.03%), 4 in pathogenic processes (1.02%) and 1 in cell adhesion (0.25%) (Fig. 11.A).

C. acnes H1 EVs contain 38 proteins involved in cellular processes (38%), 35 in metabolic processes (35%), 8 in transport (8%), 3 in biological regulation (3%) and 2 in response to stimulus (2%) (Fig. 11.B). *C. acnes* KPA EVs contain 15 proteins involved in cellular processes (35.71%), 12 in metabolic processes (28.57%), 4 in transport (9.52%) and 1 in pathogenesis (2.38%) (Fig. 11.C). Remarkably, proteins involved in pathogenic processes have only been found in A1 and KPA EVs.

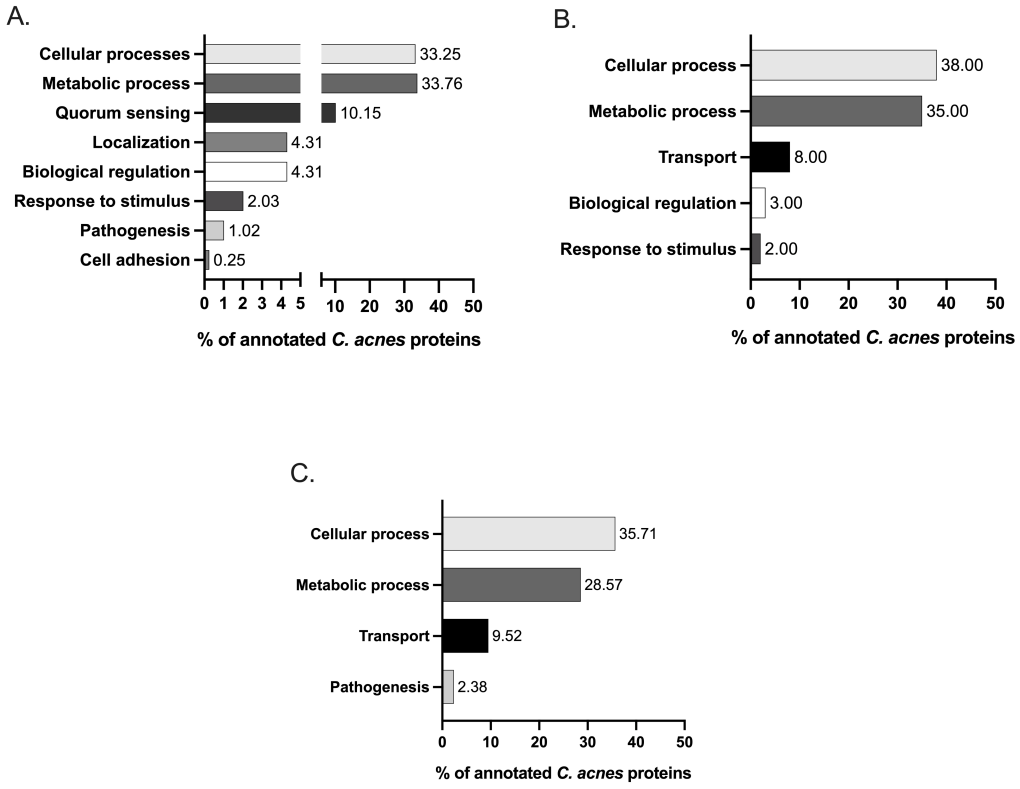

Figure 11: **Proteomic profile of *C. acnes* EVs.** Gene Ontology (GO) term of biological processes of **(A)** *C. acnes* A1 EVs, **(B)** *C. acnes* H1 EVs **(C)** and *C. acnes* KPA EVs.

The whole proteins identified are listed in Tables 3, 4 and 5 in the Supplementary Information section 7.2.2.

3.5 *In vitro* testing

3.5.1 Cytotoxicity assay

A cytotoxicity assay was performed with both immortalized cell lines: keratinocytes (HaCaT) and sebocytes (SZ95). The test was conducted only with H1 *C. acnes* EVs, as this strain is the one considered to have a protective role. The results obtained are demonstrated in Fig. 12.

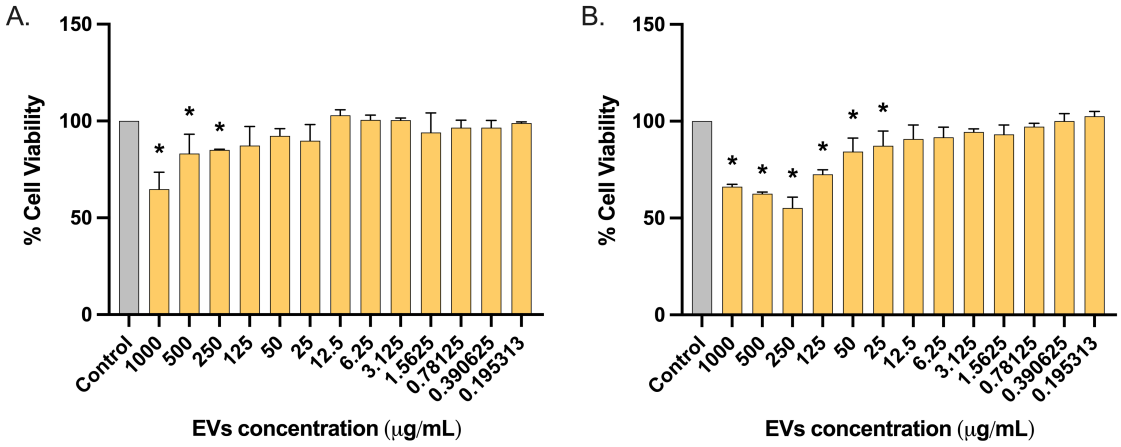

Figure 12: Cytotoxicity assay of **(A)** HaCaT cell line and **(B)** SZ95 cell line treated with different concentrations of H1 EVs. All data are presented as mean ± standard deviation (SD) of triplicate measurements ($^*p \leq 0.05$ versus non-stimulated controls).

As is shown in Fig. 12., in general, as the concentration of H1 EVs is reduced, the percentage of cell viability increases. High concentrations including 1000 and 500 μg/mL reduce cell viability to 60- 80%. However, concentrations lower than 25 μg/mL do not drastically affect cell viability as it is between 80-100% and these values could be accepted and used for the next *in vitro* experiments in the inflammatory model.

3.5.2 *C. acnes* EVs treatment

HaCaT, SZ95 and Jurkat immortalized cell lines, were used to evaluate the immunomodulatory effects of the EVs secreted by different *C. acnes* strains. Direct stimulation of these immortalized cell lines can be used as a simplified *in vitro* model of the skin. In all *in vitro* models, the cell types were stimulated by the addition of *C. acnes* EVs for 24 hours.

As illustrated in Fig. 13, all *C. acnes* EVs induce the secretion of IL-8, TGFβ-1, COX-2, CLDN-1, OCLN and MMP-2 in HaCaT cells.

Apparently, A1 EVs trigger greater activation of the proinflammatory cytokines IL-8 and TGFβ-1 and the prostagladin COX-2, than H1 and KPA EVs (Fig. 13.A).

Fig. 13.B shows that in all *C. acnes* strains, there is a significant tendency to increment the expression of CLDN-1. On the other hand, medium and high concentrations of H1 EVs (25 μg/mL and 50 μg/mL) and KPA EVs (highest peak expression at 25 μg/mL), seem to increment the expression of OCLN. Finally, when looking at the expression levels of MMP-2 (Fig. 13.B), a matrix metalloproteinase involved in tissue remodelling [27], no significant differences are found with respect to the control.

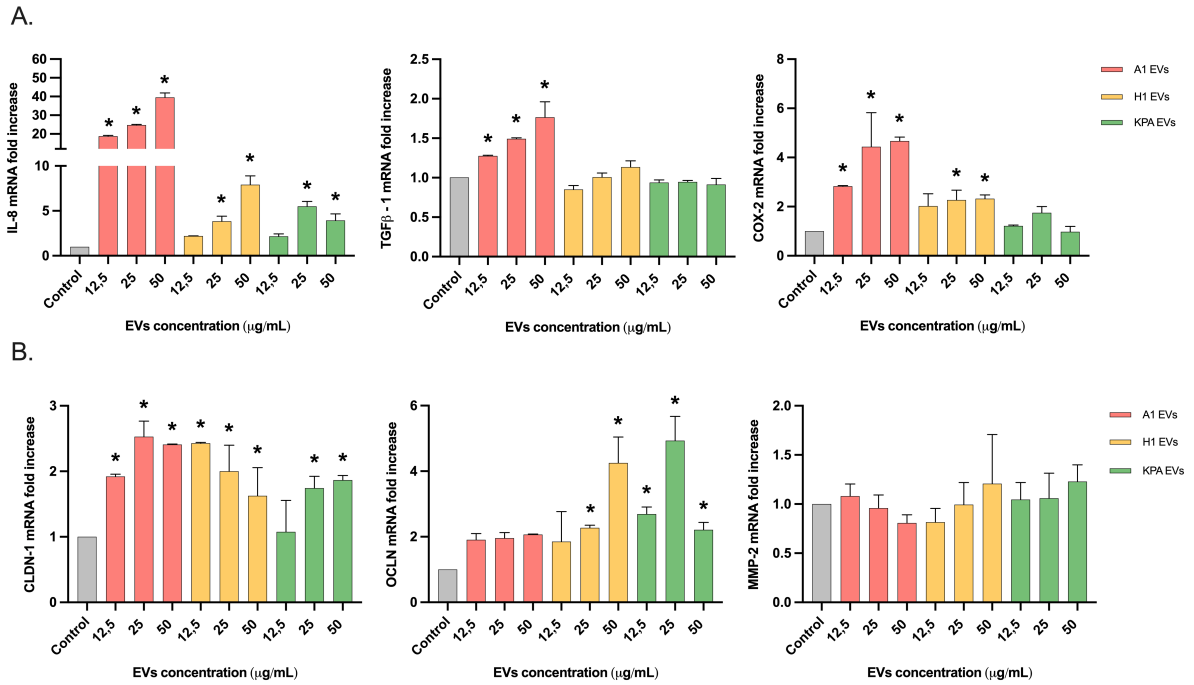

Figure 13: **Gene expression analyses in HaCaT cell line. (A)** Expression analyses of the secreted inflammatory factors IL-8, TGFβ-1 and COX-2 in HaCat cells treated with different *C. acnes* EVs. **(B)** Expression analyses of the secreted factors CLDN-1 and OCLN, involved in barrier reinforcement, and MMP-2 involved in tissue remodelling. All data are presented as mean $\pm$ standard deviation (SD) of triplicate measurements ($^*p \leq 0.05$ versus non-stimulated controls).

As illustrated in Fig. 14.A, A1 EVs are consistently triggering greater activation of inflammatory cytokines. On the other hand, Fig. 14.B shows that for A1 and KPA EVs, basal levels of PLIN-2 expression are maintained. For H1 EVs, it can be confirmed that basal levels of fat expression are even reduced. Nevertheless, most of these results are not statistically significant (p value > 0.05).

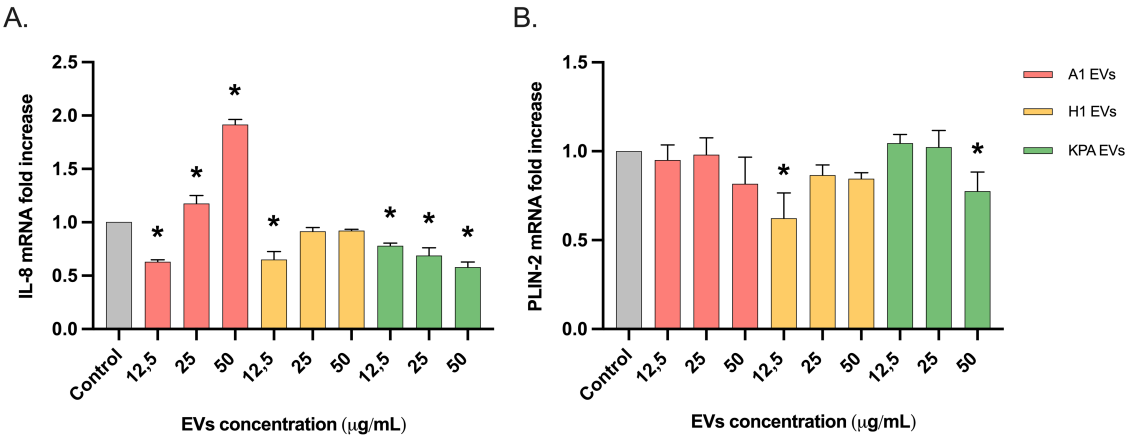

Figure 14: **Gene expression analyses in SZ95 cell line.(A)** Expression analyses of the secreted cytokine IL-8. **(B)** Expression analyses of the secreted factor PLIN-2 involved in sebum production. All data are presented as mean $\pm$ standard deviation (SD) of triplicate measurements ($^*p \leq 0.05$ versus non-stimulated controls).

As illustrated in Fig. 15, A1 EVs trigger greater activation of the proinflammatory cytokines IL-8 and TNFα whereas H1 EVs increase the expression levels of the anti-inflammatory cytokine IL-10.

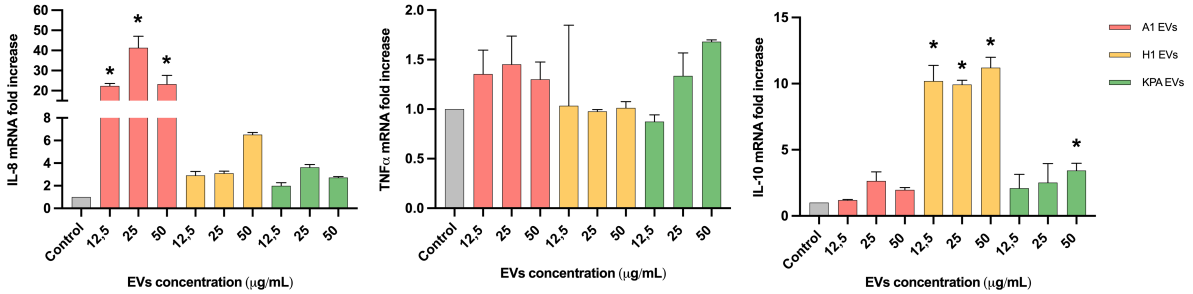

Figure 15: **Gene expression analyses in Jurkat cell line.** Expression analyses of the secreted pro-inflammatory cytokines IL-8 and TNFα and the secreted anti-inflammatory cytokine IL-10. All data are presented as mean $\pm$ standard deviation (SD) of triplicate measurements ($^*p \leq 0.05$ versus non-stimulated controls).

3.5.3 Inflammatory model

The present *in vitro* model attempts to mimic this inflammation associated with acne development. As it is illustrated in Fig. 16, there is a lot of variability in the AA assay. Although some mRNA levels are considered statistically significant, no correlation is evidenced between the amount of AA and the inflammation produced by it.

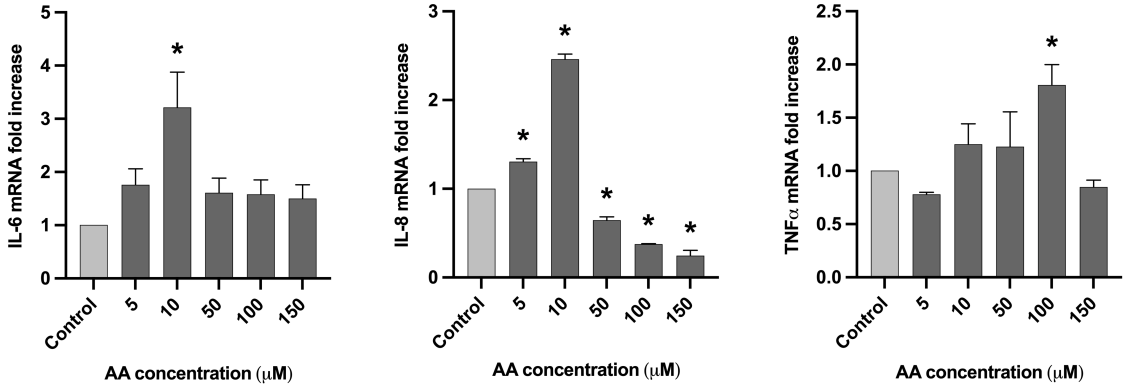

Figure 16: **HaCaT cells treated with AA.** Expression analyses of the secreted pro-inflammatory cytokines IL-6, IL-8 and TNFα. AA concentrations of 5 μM, 10 μM, 50 μM, 100 μM and 150 μM were tested during 24 hours. All data are presented as mean $\pm$ standard deviation (SD) of triplicate measurements ($^*p \leq 0.05$ versus non-stimulated controls).

Fig. 17 shows a correlation between the inflammation levels and the concentration of LPS used in HaCaT cells, with significant mRNA expression levels in all pro-inflammatory cytokines.

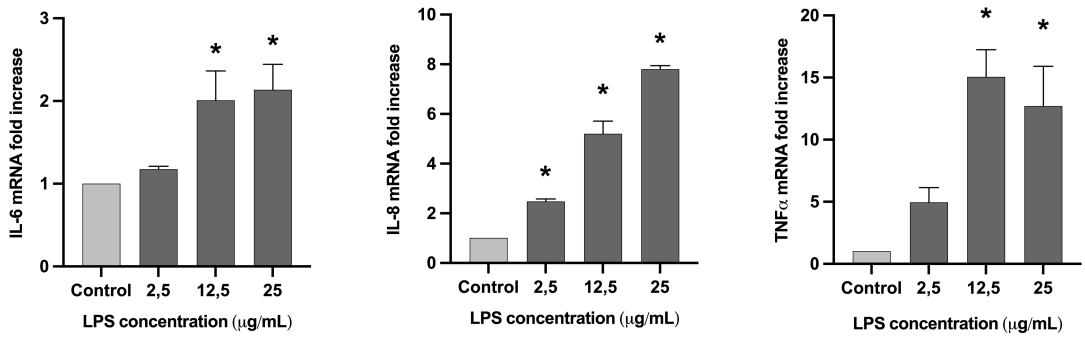

Figure 17: **HaCaT cells treated with LPS.** Expression analyses of the secreted pro-inflammatory cytokines IL-6, IL-8 and TNFα. LPS concentrations of 2.5 μg/mL, 12.5 μg/mL and 25 μg/mL were tested during 24 hours. All data are presented as mean $\pm$ standard deviation (SD) of triplicate measurements ($^*p \leq 0.05$ versus non-stimulated controls).

Fig. 18 certifies, as well, a correlation between the inflammation levels and the concentration of LPS used in SZ95 cells. Significant mRNA expression levels are only considered in IL-6 and TNFα.

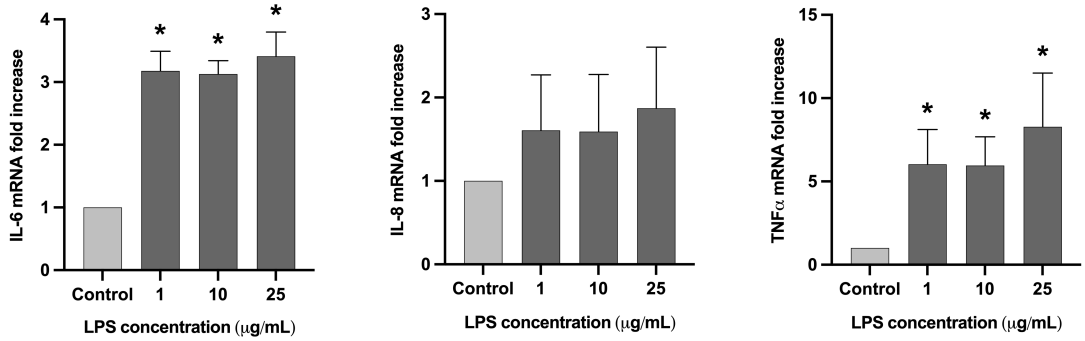

Figure 18: **SZ95 cells treated with LPS.** Expression analyses of the secreted pro-inflammatory cytokines IL-6, IL-8 and TNFα. LPS concentrations of 1 μg/mL, 10 μg/mL and 25 μg/mL were tested during 24 hours. All data are presented as mean $\pm$ standard deviation (SD) of triplicate measurements ($^*p \leq 0.05$ versus non-stimulated controls).

As it is illustrated in Fig. 19, in the PA assay there is no correlation between the inflammation levels and the concentration of PA used in SZ95 cells. No significant mRNA expression levels are substantiated in any inflammatory cytokine.

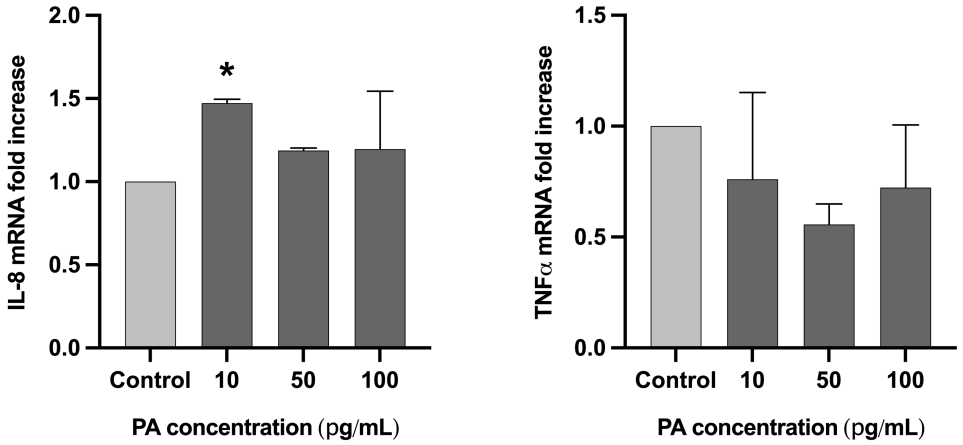

Figure 19: **SZ95 cells treated with PA.** Expression analyses of the secreted pro-inflammatory cytokines IL-6, IL-8 and TNFα. PA concentrations of 100 pg/mL, 50 pg/mL and 10 pg/mL were tested during 24 hours. All data are presented as mean $\pm$ standard deviation (SD) of triplicate measurements ($^*p \leq 0.05$ versus non-stimulated controls).

3.5.4 2D skin inflammatory model

Keratinocytes, sebocytes and lymphocytes establish a communication pathway to keep and to maintain the healthy status of the skin. In the present 2D inflammatory model the communication between HaCaT and Jurkat cells has been studied by using a Transwell System. As it can be verified in Fig. 20, inflammation was only induced for IL-8 in HaCaT cells located in the apical compartment of the co-culture.

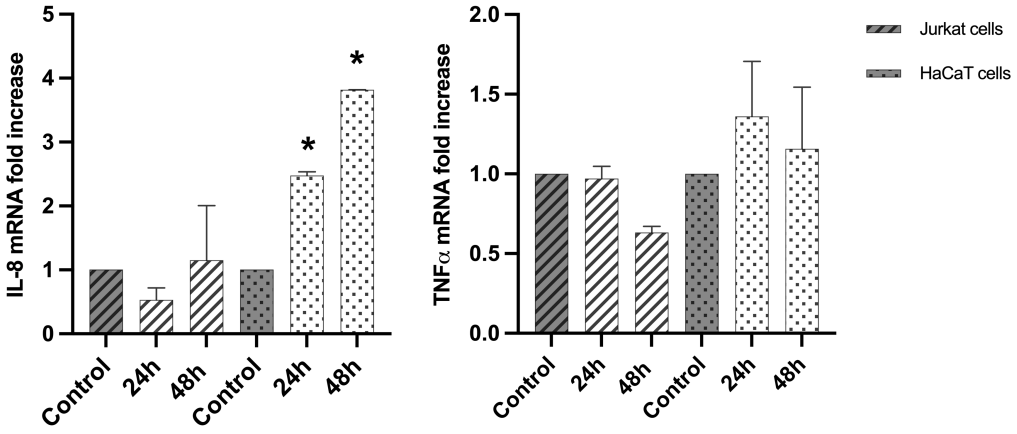

Figure 20: **Transwell System model.** Expression analyses of the secreted pro-inflammatory cytokines IL-8 and TNFα. Treated with a concentration of LPS during 24 and 48 hours. After 24 hours had passed inflammation mediated by LPS was induced using a concentration of 12.5 μg/mL. All data are presented as mean $\pm$ standard deviation (SD) of triplicate measurements ($^*p \leq 0.05$ versus non-stimulated controls).

4 Discussion

C. acnes is one of the most abundant bacterium constituting the skin microbiota. The main function of this prokaryotic outermost layer is to form an effective barrier between the organism and the environment, which effectively maintains a healthy skin status. It is well-known that both microbiota and host establish a communication mediated by EVs, nano-sized lipid bilayer vesicles constantly secreted by most cells into the extracellular environment [15]. The existence of *C. acnes* EVs is well-documented [6, 7, 14, 15, 16, 17, 18, 19], however, we wanted to corroborate our isolation method by visualizing them by TEM. For further study of *C. acnes* EVs, NTA was performed by *Institut de Ciència de materials de Barcelona*. The results obtained showed that the secretion of EVs was much higher in *C. acnes* A1 than in the other strains (see Table 1). This fact supports the hypothesis stated at the very beginning of the project, which views *C. acnes* A1 as a pathogenic strain [8]. This assumption can be made considering that, in general, pathogenic bacterial strains have an uncontrolled proliferation rate.

Once the existence of EVs in the samples was verified, a characterization of their molecular cargo was performed considering only protein and RNA content in order to shed some light on their mechanism of action.

Through RNA sequencing, two relevant human miRNAs have been found: hsa-miR-8485 and hsa-miR-10b-3p. Studies have discovered that mammalian neurotransmitters can be produced and/or consumed by several types of bacteria [28]. Furthermore, it was demonstrated that bacteria in the gut could produce many types of neurotransmitters, which mediate communication between the nervous system and the immune system [29]. In 2014, Zhen Fan et al. [30] identified the miR-8485, designated as miR-NID1, a novel miRNA that represses NRXN1 expression by binding to the Tar DNA-binding protein 43 (TDP-43). TDP-43, to binding of specific miRNAs, is involved in regulating neurotransmitters associated to neuro-developmental activities. Recently, it has been described the role of the skin microbiota controlling the brain through the secretion of neurotransmitters. The fact that EVs carry small RNAs linked to brain functions highlights the implication of EVs in the gut-brain-skin axis, a communication route thought to be involved in the modulation of neurotransmitters. In 1930, Stokes and Pillsbury [31] first proposed the gut–brain–skin axis concept, suggesting that gastrointestinal regulation mediates the influence of emotional and nervous states on the skin. On the basis of the gut–brain–skin axis theory, by understanding the communication pathways and their associations with disease, new targets, such as EVs, could be used for the treatment of skin diseases such as psoriasis and acne vulgaris. Regarding hsa-miR-10b-3p, recent studies have demonstrated its association with cerebral ischemia [32]. However, there is no information on this miRNA in the skin context. Further research is needed to clarify its role in *C. acnes* EVs.

Subsequently, proteomic profiling of *C. acnes* EVs from three different strains A1, H1 and KPA was performed and a total of 1229 proteins were identified. This was a challenging task considering that the proteome of *C. acnes* is scarcely characterized; most of the proteins are unreviewed. The Venn diagram (see Fig. 9) verified, by the high number of proteins shared, that indeed all three strains come from a single parental organism. Although they are thought to have completely opposite roles in acne development, A1 and H1 are the strains that share more proteins (13.9%). Regarding KPA, it shares approximately the same percentage of proteins with A1 (5.4%) and with H1 (5.9%), reinforcing its role as a commensal strain.

By looking at the proteins unique to each strain, the highest number of high-confidence proteins has been identified in A1 EVs (32.2%), since a larger percentage of proteins are annotated for this strain. For H1 strain, the number of high-confidence proteins identified was 100 (8.1%) and KPA was the strain with the least number of high-confidence proteins identified (3.4%). Many of these proteins have known molecular functions and are involved in biological processes as stated in the protein ID mapping website of UniProt. Thanks to UniProt database, a GO analysis was carried out and it allowed a much more detailed description of some of the proteins, by taking into account three main aspects: their molecular function, the biological processes in which they are involved and their cellular location. Considering the cellular location (see Fig. 10) a high percentage of the identified proteins were plasma membrane and cytoplasm proteins. On the other hand, proteins embedded inside the EVs seem to play important roles in transport systems and also in metabolic and cellular processes (see Fig. 11). A distinct proteomic profile is shown in terms of biological processes due to the percentage of reviewed proteins for each strain. More biological processes have been found to be associated with the proteins carried by A1 EVs, with respect to H1 and KPA, as they are better characterized.

These results emphasize the importance of such spherical vesicular structures. They are no longer considered mere cargo structures that transport information from secretory to receptor cells. EVs do act as transport carriers but they are also involved in catabolic and anabolic processes, in biological regulation, in quorum sensing, in pathogenesis, etc.

In terms of pathogenicity, certain types of skin-associated bacteria can have a virulent activity by several molecular mechanisms, including the production of biofilms and the secretion of EVs [33]. The expression of virulence factors has as main functions, triggering immune responses in the host and/or promoting the adaptation of *C. acnes* to its environment [34]. Interestingly, one pathogenic protein has been identified in KPA EVs; an extracellular region protein called endo-beta-N-acetylglucosaminidase H, which is involved in metabolizing host tissue-derived substrates [14]. On the other hand, EVs secreted by *C. acnes* A1 also contained proteins involved in pathogenic processes such as hyaluronate lyase, triacylglycerol lipase, glycosyl hydrolase and phospoesterase. Hyaluronate lyase is an enzyme found predominantly in Gram-positive bacteria, especially in those that inhabit or are pathogenic on the skin [35]. It hydrolyzes the extracellular matrix between mammalian host cells. Degraded extracellular matrix fragments (hyaluronan fragments) have been reported to act as an endogenous danger signal, leading to the activation of both innate and acquired immunity [14, 36]. Triacylglycerol lipase, also designated as glycerol-ester hydrolase A (GehA), is recognized as one of the virulence factors involved in the pathogenesis of acne. It is the responsible of the hydrolysis of sebum triacylglycerides which results in the release of glycerol and free fatty acids. These fatty acids are considered inflammatory, promoting acne-like phenotypes [37, 38, 39]. The glycosyl hydrolase is an enzyme involved in cell wall macromolecule catabolic processes and peptidoglycan catabolic processes. The ability to degrade peptidoglycans may serve as a means of nutrition for *C. acnes* A1 and possibly, facilitate the colonization of the skin and contribute to acne development in susceptible individuals [40]. Additionally, the phospoesterase is an enzyme which has hydrolase activity acting on ester bonds, and it has been classified as virulent, however a more complete knowledge of its biochemical characteristics is needed in order to validate its skin pathogenesis.

In parallel, different *in vitro* models were developed in order to mimic the human skin. As previously mentioned, *C. acnes* is one of the most predominant bacterium within the skin microbiome; it colonizes the skin surface and it is in direct contact with keratinocytes. Also, under healthy skin conditions the skin barrier is intact and commensal bacteria can not have access to deeper layers of the skin where sebocytes (specifically isolated by sebum) or lymphocytes inhabit. However, it is known that all of them establish a communication pathway to maintain the healthy status of the skin. This communication is mediated by EVs, small particles able to be internalized [41]. In this context, to mimic the main cell types of the skin, three cell lines have been selected: HaCaT, SZ95 and Jurkat. These immortalized cell lines were used to mimic, in a simplified way, all the cell types present in the skin and the interactions established between them (Fig. 21).

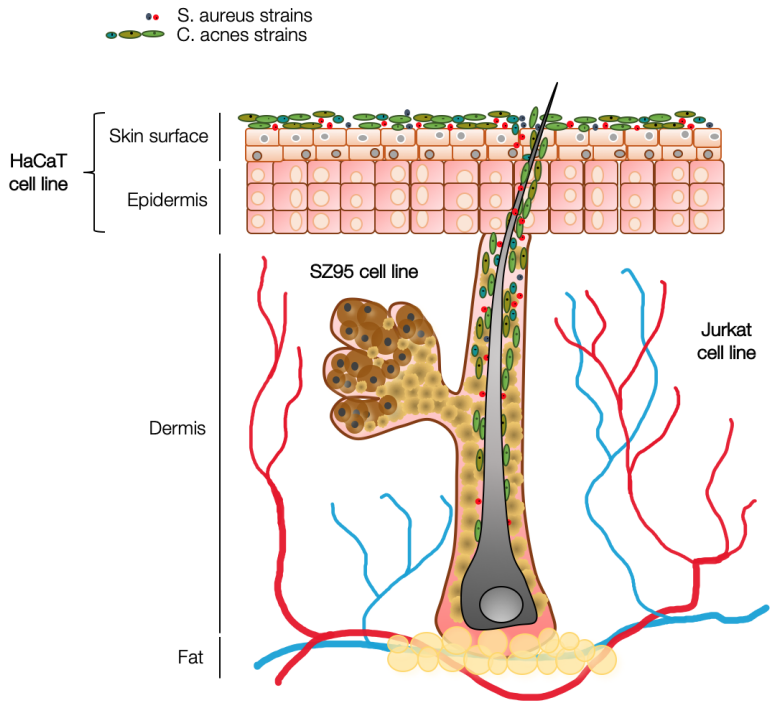

Figure 21: Representation of the different skin layers including the specific cell lines used in this project.

The first step for *in vivo* tests was to assess the optimal concentration of EVs that was not having a cytotoxicity effect on HaCaT and SZ95 cell lines. In HaCaT, concentrations lower than 250 μg/mL did not reduce cell viability. On the other hand, concentrations of EVs lower than 25 μg/mL were found to be safe for the SZ95 cell line thus, appropriate to use in subsequent studies. This fact may be because HaCaT are in direct contact with skin bacteria and are therefore already sensitized to bacterial components. However, this is not the case for SZ95 as they are protected by a layer of sebum and bacteria and, under normal conditions, are not in contact with them [2]. Due to this, SZ95 cell line might be more sensitive even at lower concentrations. In any case, even when testing high concentrations of EVs, cell viability was reduced by more than 50%. Overall, this test showed that EVs, applied in a concentration lower than 25 μg/mL, were not harmful and they can be safely applied topically. However, some scientific publications advise researchers not to rely only in MTT assays to estimate viability and infer cytotoxic effects [42, 43].

They suggest to verify cell viability and proliferation with additional experimental assays such as cell membrane damage assays [43]. This information indicates that perhaps, in the future, more sophisticated tests should be carried out to have much more accurate viability results.

After that, EVs were incubated directly with the different immortalized cell lines: HaCaT, SZ95 and Jurkat. Results showed that, in all models, A1 EVs were consistently triggering greater activation of inflammatory cytokines rather than H1 and KPA EVs. In the HaCaT model, apart from inflammatory mediators, barrier reinforcement (CLDN-1 and OCLN) factors were tested (see Fig. 13.B). Regarding OCLN mRNA expression, concentrations of 50 μg/mL for H1 EVs and of 25 μg/mL for KPA EVs were considered as optimal concentrations to reinforce the epithelial barrier. However, for the rest of conditions, no statistically significant results were obtained, suggesting that these assays should be repeated using different concentrations of EVs at different time points. Moreover, in this model, the expression of one tissue remodeling mediator (MMP-2) was assessed (see Fig. 13.B). It is predicted that longer incubation of HaCaT cells with *C. acnes* EVs would show a clearer trend in the expression levels of this gene involved in cutaneous wound healing. This fact could be assumed since it has been shown that MMP-2 expression after skin injury reaches the highest level around days 5-7 post-wounding, whereas in the present project the incubation of EVs was only 24 hours [34]. In the SZ95 model, the 24-hour incubation with H1 EVs resulted in a slightly reduction of PLIN-2 expression, which is related with a decrease in sebum production (see Fig. 14.B). Nevertheless, to obtain reliable data, these results need to be repeated including other genes implicated in the production of sebum. In the Jurkat model the anti-inflammatory cytokine IL-10 was studied after 24 hours of incubation with the immortalized T lymphocytes cell line. The results obtained showed that H1 EVs increased significantly mRNA expression levels of IL-10 (see Fig. 15). These findings supported the hypothesis that H1 *C. acnes* strain has a protective role, in this case by counteracting inflammation.

As is well-known, acne vulgaris is associated with excess sebum production, hyperkeratinization and production of inflammatory mediators. These inflammatory mediators induce keratinocyte proliferation, which may contribute to follicular occlusion and enhanced sebum retention. In the *in vitro* skin inflammatory model, several inflammatory agents (AA, PA and LPS) were evaluated based on previous bibliography research. For AA a range between 5-150 μM of AA was incubated in HaCaT for 24 hours. The 10 μM concentration was the only one that increased IL-6 and IL-8 expression and similarly, 100 μM was the only inducing TNFα mRNA expression. Moreover, the fold increase ratios obtained for the three pro-inflammatory cytokines were not good enough compared to previous published studies, probably due to AA fatty acid nature that makes it very hard to get homogeneous solutions to work with. Therefore, this model was discarded.

In the PA model [44], lower concentrations of this saturated fatty acid, from 10 to 100 pg/mL, were tested on SZ95 cell line for 24 hours. Since sebocytes are much more sensible than keratinocytes, a clear inflammation pattern was expected to be seen. Nevertheless, the inflammation produced by PA was not enough to simulate an acne-prone skin. Therefore, this model was also discarded.

In the LPS *in vitro* inflammatory model, both HaCaT and SZ95 cell lines were used [45, 46, 47]. Opposite to the previous models, LPS did stimulate the pro-inflammatory cytokines IL-6 and TNFα compared to the negative control. Thus, a concentration of 12.5 μg/mL was the one selected to be used in the 2D inflammatory skin model.

Subsequently, inflammation was tried to be induced in a co-culture model of keratinocytes (HaCaT) and T lymphocytes (Jurkat). HaCaT cells were seeded in the apical compartment of the Transwell system and Jurkat cells in the basolateral compartment. To determine which condition induced inflammation in the whole system, LPS was incubated in the apical compartment for 24 and 48 hours. In both cases, for HaCaT, inflammation was induced increasing IL-8 and TNFα gene expression (see Fig. 20). However, for Jurkat there was no inflammation in any of the time-points tested. Different times of incubation and LPS concentrations need to be tested in order to establish a whole *in vitro* inflammation system.

As specified before, further studies are needed to refine the project idea. However, during this short period of time we have had to face different challenges. *C. acnes* is an anaerobic, Gram-positive bacterium with a relatively slow-growing rate. It needs at least 10 days to grow in 1L culture bottles in anaerobic conditions; a limiting factor throughout the project. Currently, EVs isolation gold standard is the ultracentrifugation method; nevertheless, this method is time-consuming and tedious, mainly because of the duration of the centrifugation runs, which require large volumes of culture to overcome the low yields of EVs naturally produced by cultured bacteria. In addition, new protocols had to be established in the laboratory for the RNA sequencing analysis and for the sample preparation and analysis for proteomics and last but not least, a 2D skin model was developed *de novo*.

Nonetheless, the results presented in the present project, provide useful evidence for a better understanding of the biological and pathophysiological mechanisms of *C. acnes* EVs. Additionally, EVs are non-replicative, stable structures which have the capacity to remodel both proximal and distal epithelial cells. For this reason, EVs could be ideal probiotic substitutes with a higher and more targeted therapeutic potential.

This work could be considered as a step forward for the safe translation of EV-based therapies into clinical practice.

5 Conclusions

C. acnes EVs can be isolated from 1L cultured medium following the previously described ultracentrifugation-filtration process. However the yield is very low due to the slow growing rate of this bacterium (10 days). *C. acnes* EVs can be visualized by TEM but also by NTA techniques and it has been annotated that A1, H1 and KPA have an average mean size of 96.8, 100.7 and 133 respectively. Furthermore, small RNA sequencing analysis of *C. acnes* EVs unveiled that these particles are charged with miRNAs from human; being hsa-miR-8485 the most expressed one. However, more exhaustive data processing is needed to know which bacterial *de novo* miRNAs are loaded in EVs and their target genes. Proteomic analysis of *C. acnes* EVs revealed that A1 and KPA nano-sized particles are loaded with pathogenicity-associated proteins whereas H1 is not; confirming the published non-pathogenic profile of this bacterium in contrast to the others [1]. Nonetheless, a large percentage of proteins mainly for KPA and H1 are not annotated in the UniProt data base. On the other hand, the *in vitro* cytotoxicity test performed with H1 EVs in SZ95 (sebocytes) and HaCaT (keratinocytes) models determined that concentrations lower than 50 μg/mL reduce cell viability by less than 20% and they can be safely used for topical administration.

C. acnes A1, H1 and KPA were tested in HaCaT, SZ95 and JurKat *in vitro* models. Direct incubation in HaCaT cells showed, for A1, a higher expression of the pro-inflammatory biomarkers (IL-8, TGFβ-1 and COX-2) and that only H1 and KPA were able to upregulate CLDN-1 and OCLN genes related to skin barrier maintaining. SZ95 and Jurkat EVs incubations also confirmed the inflammatory trend of A1 EVs increasing IL-8. Moreover, in the Jurkat model only H1 EVs upregulated the anti-inflammatory IL-10. All these data pointed to the beneficial effect of H1 EVs in contrast to A1 or KPA EVs. The inflammatory *in vitro* model was assayed with AA, PA and LPS, but only LPS was able to increase pro-inflammatory genes in a significantly way. However, when it was tested at 12.5 μg/mL in a 2D Transwell System formed by HaCaT and Jurkat cells, the inflammatory signal did not reach to the basolateral lymphocytes. Therefore, more experiments need to be done in order to optimize the *in vitro* inflammatory 2D system.

6 Future work

Further testing is needed in order to obtain a consistent characterization of *C. acnes* EVs. Aware of it, different future approaches are proposed.

To complete the RNA sequencing analysis, a comprehensive *de novo* sequencing approach needs to be conducted in order to identify new miRNAs embedded inside the EVs. Moreover, their target genes should be determined so that the most abundant miRNAs could be validated by RT-qPCR.

To get the most out of the proteomic analysis results, it would be interesting to compare the proteomic profile of the *C. acnes* bacterium itself versus the proteomic profile of its EVs. This comparison would allow us to determine whether the EVs encapsulate proteins through a random process or whether it is a process delivered by environmental conditions.

On the other hand, due to the unresponsive *in vitro* results obtained in our inflammatory model, a collaboration has been established with the French company Phenocell SAS, as they work with sebocytes and keratinocytes primary cell lines and they have an already established protocol for inflammation with AA. The different *C. acnes* EVs will be tested following their model in order to characterize the immunomodulatory role that EVs play in a damaged skin tissue environment.

When considering using vesicles as a delivery method, another potential approach is the *ex-vivo* modification of these EVs in order to load them, for instance, with therapeutic molecules. EVs have been previously loaded with siRNAs via electroporation [48, 49] which suggests that *C. acnes* EVs could be electroporated and loaded with small molecule drugs to modulate expression of inflammatory targets in the host.

To finish, selected EVs conditions with promising therapeutic effects will be tested, by topical administration, in an *in vivo* model closer to reality taking as reference other already described mouse models of atopic dermatitis (AD) [50] and inflammatory acne-like lesions [51].

Bibliography

[1] Paetzold B. et al. "Skin microbiome modulation induced by probiotic solutions." In: *Microbiome* 7).1 (2019), p. 95. DOI: https://doi.org/10.1186/s40168-019-0709-3.

[2] Lawton S. "Skin 1: the structure and functions of the skin." In: *Nursing times (online)* 115.12 (2019), pp. 30–33.

[3] Grice E. and Segre J. "The skin microbiome." In: *Nature reviews. Microbiology* 9.4 (2011), pp. 244–253. DOI: https://doi.org/10.1038/nrmicro2537.

[4] Eisenstein M. "The skin microbiome." In: *Nature* 588.7838 (2020). DOI: https://doi.org/10.1038/d41586-020-03523-7.

[5] Segre J. et al. "The human skin microbiome". In: *Nature Reviews Microbiology* 16.3 (2018), pp. 143–155. DOI: https://doi.org/10.1038/nrmicro.2017.157.

[6] Fitz-Gibbon S. et al. "Propionibacterium acnes strain populations in the human skin microbiome associated with acne." In: *Invest Dermatol* 133.9 (2013), pp. 2152–2160. DOI: https://doi.org/10.1038/jid.2013.21.

[7] McLaughlin J et al. "Propionibacterium acnes and Acne Vulgaris: New Insights from the Integration of Population Genetic, Multi-Omic, Biochemical and Host-Microbe Studies." In: *Microorganisms* 7.5 (2019), p. 128. DOI: https://doi.org/10.3390/microorganisms7050128.

[8] O'Neill AM and Gallo RL. "Host-microbiome interactions and recent progress into understanding the biology of acne vulgaris." In: *Microbiome* 6.1 (2018), p. 177. DOI: https://doi.org/10.1186/s40168-018-0558-5.

[9] Seth D. and Cheldize K. "Global Burden of Skin Disease: Inequities and Innovations." In: *Current Dermatology Reports* 6.3 (), pp. 204–210. DOI: https://doi.org/10.1007/s13671-017-0192-7.

[10] Bhate K and Williams HC. "Epidemiology of acne vulgaris." In: *The British journal of dermatology* 168.3 (2013), pp. 474–485. DOI: https://doi.org/10.1111/bjd.12149.

[11] Dalgard F. et al. "Self-esteem and body satisfaction among late adolescents with acne: Results from a population survey." In: *Journal of the American Academy of Dermatology* 59.5 (2008), pp. 746–751. DOI: https://doi.org/10.1016/j.jaad.2008.07.013.

[12] Halvorsen Jon A et al. "Suicidal ideation, mental health problems, and social impairment are increased in adolescents with acne: a population-based study." In: *The Journal of investigative dermatology* 131.2 (2011), pp. 363–370. DOI: https://doi.org/10.1038/jid.2010.264.

[13] Kilian M. Lomholt HB. "Population Genetic Analysis of Propionibacterium acnes Identifies a Subpopulation and Epidemic Clones Associated with Acne." In: *PLoS One* 5.8 (2010), e12277. DOI: https://doi.org/10.1371/journal.pone.0012277.

[14] Jeon J. et al. "Proteomic analysis of extracellular vesicles derived from Propionibacterium acnes." In: *Proteomics. Clinical applications* 11.1-2 (2017). DOI: https://doi.org/10.1002/prca.201600040.

[15] Choi EJ. et al. "Propionibacterium acnes-Derived Extracellular Vesicles Promote Acne-Like Phenotypes in Human Epidermis." In: *Journal of Investigative Dermatology.* 138.6 (2018), pp. 1371–1379. DOI: https://doi.org/10.1016/j.jid.2018.01.007.

[16] Bajic SS. et al. "Proteomic profile of extracellular vesicles released by Lactiplantibacillus plantarum BGAN8 and their internalization by non-polarized HT29 cell line." In: *Scientific Reports* 10.21829 (2020). DOI: https://doi.org/10.1038/s41598-020-78920-z.

[17] Choi DS. and Gho YS. "Isolation of Extracellular Vesicles for Proteomic Profiling." In: *Methods in Molecular Biology* (2015), pp. 167–177. DOI: https://doi.org/10.1007/978-1-4939-2550-6_14.

[18] Rontogianni S. et al. "Proteomic profiling of extracellular vesicles allows for human breast cancer subtyping." In: *Communications Biology* 2.325 (2019). DOI: https://doi.org/10.1038/s42003-019-0570-8.

[19] Quiroz-Baez R. et al. "Insights Into the Proteomic Profiling of Extracellular Vesicles for the Identification of Early Biomarkers of Neurodegeneration." In: *Frontiers in neurology* 11.580030 (2020). DOI: https://doi.org/10.3389/fneur.2020.580030.

[20] Valadi H. et al. "Exosome-mediated transfer of mRNAs and microRNAs is a novel mechanism of genetic exchange between cells." In: *Nature cell biology* 9.6 (2007), pp. 654–659. DOI: https://doi.org/10.1038/ncb1596.

[21] Heon-Jin. Lee. "Microbe-Host Communication by Small RNAs in Extracellular Vesicles: Vehicles for Transkingdom RNA Transportation." In: *International journal of molecular sciences* 20.6 (2019), p. 1487. DOI: https://doi.org/10.3390/ijms20061487.

[22] Aguilera L. et al. "Proteomic analysis of outer membrane vesicles from the probiotic strain Escherichia coli Nissle 1917." In: *Proteomics* 14.2-3 (2014), pp. 222–229. DOI: https://doi.org/10.1002/pmic.201300328.

[23] Reimer Shelby L. et al. "Comparative Analysis of Outer Membrane Vesicle Isolation Methods With an Escherichia coli tolA Mutant Reveals a Hypervesiculating Phenotype With Outer-Inner Membrane Vesicle Content." In: *Frontiers in Microbiology* 12 (2021), p. 383. DOI: https://doi.org/10.3389/fmicb.2021.628801.

[24] Hess J.F. et al. "Library preparation for next generation sequencing: A review of automation strategies". In: *Biotechnology Advances* 41.2-3 (2020). DOI: https://doi.org/10.1016/j.biotechadv.2020.107537.

[25] Chettimada S. et al. "Small RNA sequencing of extracellular vesicles identifies circulating miRNAs related to inflammation and oxidative stress in HIV patients." In: *Biotechnology Advances* 21 (1).57 (2020). DOI: https://doi.org/10.1186/s12865-020-00386-5.

[26] Potla P. et al. "A bioinformatics approach to microRNA-sequencing analysis." In: *Osteoarthritis and Cartilage Open* 3.1 (2021). DOI: https://doi.org/10.1016/j.ocarto.2020.100131.

[27] Manuel J.A. and Gawronska-Kozak B. "Matrix metalloproteinase 9 (MMP-9) is upregulated during scarless wound healing in athymic nude mice." In: *Journal of the International Society for Matrix Biology* 25.8 (2006), pp. 505–514. DOI: https://doi.org/10.1016/j.matbio.2006.07.008.

[28] Strandwitz P. "Neurotransmitter modulation by the gut microbiota." In: *Brain research* 1693.Pt B (2018), pp. 128–133. DOI: https://doi.org/10.1016/j.brainres.2018.03.015.

[29] Chen G. et al. "Gut–Brain–Skin Axis in Psoriasis: A Review." In: *Dermatol Ther (Heidelb)* 11 (2020), pp. 25–38. DOI: https://doi.org/10.1007/s13555-020-00466-9.

[30] Fan Z. et al. "Transcriptome-wide analysis of TDP-43 binding small RNAs identifies miR-NID1 (miR-8485), a novel miRNA that represses NRXN1 expression." In: *Genomics* 103.1 (2014), pp. 76–82. DOI: https://doi.org/10.1016/j.ygeno.2013.06.006.

[31] Stokes J. and Pillsbury D. "The effect on the skin of emotional and nervous states: III. Theoretical and practical consideration of a gastro-intestinal mechanism." In: *Archives of Dermatology* 22 (1930), pp. 962–993. DOI: doi:10.1001/archderm.1930.01440180008002.

[32] Duan X. et al. "Identification and functional analysis of microRNAs in rats following focal cerebral ischemia injury." In: *Molecular medicine reports* 19.5 (2019), pp. 4175–4184. DOI: https://doi.org/10.3892/mmr.2019.10073.

[33] Yoon H. et al. "Discovery of Salmonella virulence factors translocated via outer membrane vesicles to murine macrophages." In: 79.6 (2011), pp. 2182–2192. DOI: https://doi.org/10.1128/IAI.01277-10.

[34] Mayslich C. et al. "Cutibacterium acnes as an Opportunistic Pathogen: An Update of Its Virulence-Associated Factors." In: *Microorganisms* 9.2 (2021), p. 303. DOI: https://doi.org/10.3390/microorganisms9020303.

[35] Steiner B. et al. "Cloning and sequencing of the hyaluronate lyase gene from Propionibacterium acnes." In: *Canadian journal of microbiology* 43.4 (1997), pp. 315–321. DOI: https://doi.org/10.1139/m97-044.

[36] Scheibner K.A. et al. "Hyaluronan fragments act as an endogenous danger signal by engaging TLR2." In: *Journal of immunology* 177.2 (2006), pp. 1272–1281. DOI: https://doi.org/10.4049/jimmunol.177.2.1272.

[37] Miskin James E. et al. "Propionibacterium acnes, a resident of lipid-rich human skin, produces a 33 kDa extracellular lipase encoded by gehA." In: *Microbiology* 143.5 (1997), pp. 1745–1755. DOI: https://doi.org/10.1099/00221287-143-5-1745.

[38] Falcocchio S. et al. "Propionibacterium acnes GehA lipase, an enzyme involved in acne development, can be successfully inhibited by defined natural substances." In: *Journal of Molecular Catalysis B: Enzymatic* 40 (2006), pp. 132–137. DOI: https://doi.org/10.1016/j.molcatb.2006.02.011.

[39] Holland C. et al. "Proteomic identification of secreted proteins of Propionibacterium acnes". In: *BMC Microbiology* 10.230 (2010). DOI: https://doi.org/10.1186/1471-2180-10-230.

[40] Reichenbach T. et al. "Structural and biochemical characterization of the Cutibacterium acnes exo-β-1,4-mannosidase that targets the N-glycan core of host glycoproteins." In: *PloS one* 13.9 (2018), e0204703. DOI: https://doi.org/10.1371/journal.pone.0204703.

[41] Reclusa P. et al. "Improving extracellular vesicles visualization: From static to motion." In: *Scientific Reports* 10.6494 (2020). DOI: https://doi.org/10.1038/s41598-020-62920-0.

[42] van Tonder A. et al. "Limitations of the 3-(4,5-dimethylthiazol-2-yl)-2,5-diphenyl-2H-tetrazolium bromide (MTT) assay when compared to three commonly used cell enumeration assays." In: *BMC research notes* 8.87 (2015). DOI: https://doi.org/10.1186/s13104-015-1000-8.

[43] Shuguang W. et al. "Limitation of the MTT and XTT assays for measuring cell viability due to superoxide formation induced by nano-scale TiO_2." In: *Scientific Reports* 25.8 (2011), pp. 2147–2151. DOI: https://doi.org/10.1016/j.tiv.2011.07.007.

[44] Zhou Bing-rong et al. "Palmitic acid induces production of proinflammatory cytokines interleukin-6, interleukin-1β, and tumor necrosis factor-α via a NF-κB - dependent mechanism in HaCaT keratinocytes." In: 2013.530429 (2013). DOI: https://doi.org/10.1155/2013/530429.

[45] He Yuzhu et al. "The Protective Role of Feruloylserotonin in LPS-Induced HaCaT Cells". In: *Molecules (Basel, Switzerland)* 24.17 (2019). DOI: https://doi.org/10.3390/molecules24173064.

[46] Song Y. et al. "Emodin protects against lipopolysaccharide-induced inflammatory injury in HaCaT cells through upregulation of miR-21." In: *Artificial Cells, Nanomedicine, and Biotechnology* 41.1 (2019), pp. 2654–2661. DOI: https://doi.org/10.1080/21691401.2019.1629951.

[47] Li S. et al. "Schizandrin A Alleviates LPS-Induced Injury in Human Keratinocyte Cell Hacat Through a MicroRNA-127-Dependent Regulation." In: *Cellular physiology and biochemistry: international journal of experimental cellular physiology, biochemistry, and pharmacology.* 49.6 (2018), pp. 2229–2239. DOI: https://doi.org/10.1159/000493826.

[48] Lamichhane T. N. and Jay S. M. "Production of Extracellular Vesicles Loaded with Therapeutic Cargo". In: *Methods in molecular biology (Clifton, N.J.)* 1831 (2018), pp. 37–47. DOI: https://doi.org/10.1007/978-1-4939-8661-3_4.

[49] Kooijmans Sander A A et al. "Electroporation-induced siRNA precipitation obscures the efficiency of siRNA loading into extracellular vesicles." In: *Journal of controlled release: official journal of the Controlled Release Society* 172.1 (2013), pp. 229–238. DOI: https://doi.org/10.1016/j.jconrel.2013.08.014.

[50] Kitamura A. et al. "A murine model of atopic dermatitis can be generated by painting the dorsal skin with hapten twice 14 days apart." In: *Scientific Reports volume* 8.5988 (2018). DOI: https://doi.org/10.1038/s41598-018-24363-6.

[51] Jang Yong Hyun et al. "HR-1 Mice: A New Inflammatory Acne Mouse Model." In: *Annals of dermatology* 27.3 (2015), pp. 257–264. DOI: https://doi.org/10.5021/ad.2015.27.3.257.

[52] Chiva C. et al. "A cloud-based quality control system for mass spectrometry-based proteomics laboratories." In: *PLoS One* 13.1 (2018), e0189209. DOI: https://doi.org/10.1371/journal.pone.0189209.

[53] Perkins D.N. et al. "Probability-based protein identification by searching sequence databases using mass spectrometry data." In: *Electrophoresis* 20.18 (1999), pp. 3551–3567. DOI: https://doi.org/10.1002/(SICI)1522-2683(19991201)20:18<3551::AID-ELPS3551>3.0.CO;2-2.

[54] Beer Lynn A. et al. "Efficient quantitative comparisons of plasma proteomes using label-free analysis with MaxQuant." In: *Methods Molecular Biology* 1619 (2017), pp. 339–352. DOI: https://doi.org/10.1007/978-1-4939-7057-5_23.

7 Supplementary information

7.1 Methods

7.1.1 Purification of EVs total protein: Proteomic analysis

Sample preparation

Samples (8 μg) were reduced with dithiothreitol (24 nmol, 37°C, 60 min) and alkylated in the dark with iodoacetamide (48 nmol, 25°C, 30 min). The resulting protein extract was first diluted to 2M urea with 200 mM ammonium bicarbonate for digestion with endoproteinase LysC (1:10 w:w, 37°C, o/n, Wako, cat # 129-02541), and then diluted 2-fold with 200 mM ammonium bicarbonate for trypsin digestion (1:10 w:w, 37°C, 8h, Promega cat # V5113). After digestion, peptide mix was acidified with formic acid and desalted with a MicroSpin C18 column (The Nest Group, Inc) prior to LC-MS/MS analysis.

Chromatographic and mass spectrometric analysis

Samples were analyzed using a LTQ - Orbitrap Fusion Lumos mass spectrometer (Thermo Fisher Scientific, San Jose, CA, USA) coupled to an EASY-nLC 1200 (Thermo Fisher Scientific (Proxeon), Odense, Denmark). Peptides were loaded directly onto the analytical column and were separated by reversed-phase chromatography using a 50-cm column with an inner diameter of 75 μm, packed with 2 μm C18 particles spectrometer (Thermo Scientific, San Jose, CA, USA).

Chromatographic gradients started at 95% buffer A and 5% buffer B with a flow rate of 300 nl/min for 5 minutes and and gradually increased to 25% buffer B and 75% A in 79 minutes and then to 40% buffer B and 60% A in 11 minutes. After each analysis, the column was washed for 10 minutes with 10% buffer A and 90% buffer B. Buffer A: 0.1% formic acid in water. Buffer B: 0.1% formic acid in 80% acetonitrile.

The mass spectrometer was operated in positive ionization mode with nanospray voltage set at 2.4 kV and source temperature at 305°C. The acquisition was performed in data-dependent acquisition (DDA) mode and full MS scans with 1 micro scans at resolution of 120,000 were used over a mass range of m/z 350-1400 with detection in the Orbitrap mass analyzer, auto gain control (AGC) was set to "Standard" and maximum injection time to "Auto". In each cycle of data-dependent acquisition analysis, following each survey scan, the most intense ions above a threshold ion count of 10000 were selected for fragmentation. The number of selected precursor ions for fragmentation was determined by the "Top Speed" acquisition algorithm and a dynamic exclusion of 60 seconds. Fragment ion spectra were produced via high-energy collision dissociation (HCD) at normalized collision energy of 28% and they were acquired in the ion trap mass analyzer. AGC was set to 2E4, and an isolation window of 0.7 m/z and a maximum injection time of 12 ms were used. Digested bovine serum albumin (New England biolabs cat # P8108S) was analyzed between each sample to avoid sample carryover and to assure stability of the instrument and QCloud [52] has been used to control instrument longitudinal performance during the project.

Data Analysis

Acquired spectra were analyzed using the Proteome Discoverer software suite (v2.0, Thermo Fisher Scientific) and the Mascot search engine (v2.6, Matrix Science [53]). The data were searched against a Swiss-Prot *Cutibacterium acnes (Propionibacterium acnes)* database (as in July 20, 19.374 entries) plus a list [54] of common contaminants and all the corresponding decoy entries. For peptide identification a precursor ion mass tolerance of 7 ppm was used for MS1 level, trypsin was chosen as enzyme, and up to three missed cleavages were allowed. The fragment ion mass tolerance was set to 0.5 Da for MS2 spectra. Oxidation of methionine and N-terminal protein acetylation were used as variable modifications whereas carbamidomethylation on cysteines was set as a fixed modification. False discovery rate (FDR) in peptide identification was set to a maximum of 5%. Peptide quantification data were retrieved from the "Precursor ion area detector" node from Proteome Discoverer (v2.0) using 2 ppm mass tolerance for the peptide extracted ion current (XIC). The obtained values were used to calculate protein fold-changes and their corresponding adjusted p-values.

7.1.2 Real time quantitative PCR analysis (RT-qPCR)

Genes		**Primers (5' → 3')**
CREBBP	FWD RV	GAGAGCAAGCAAACGGAGAG AAGGGAGGCAAACAGGACA
TNFα SEB	FWD RV	CCAGGGACCTCTCTCTAATCA TCAGCTTGAGGGTTTGCTAC
IL-6 SEB	FWD RV	ACTCACCTCTTCAGAACGAATTG AGCCATCTTTGGAAGGTTCAG
IL-8 SEB	FWD RV	CTTGGCAGCCTTCCTGATTT GGGTGGAAAGGTTTGGAGTATG
PLIN2	FWD RV	TCAGCTCCATTCTACTGTTCACC CCTGAATTTTCTGATTGGCACT
TGFβ	FWD RV	TACCTGAACCCGTGTTGCTCTC GTTGCTGAGGTATCGCCAGGAA
COX-2	FWD RV	GAATCATTCACCAGGCAAATTG TCTGTACTGCGGGTGGAACA
OCLN	FWD RV	GTCATCCAGGCCTCTTGAAA GGTGATAATGATTCGGTTTG
CLDN1	FWD RV	GTCTTTGACTCCTTGCTGAATCTG CACCTCATCGTCTTCCAAGCAC
MMP2	FWD RV	AGCGAGTGGATGCCGCCTT CATTCCAGGCATCTGCGAT
IL-10	FWD RV	TCTCCGAGATGCCTTCAGCAGA TCAGACAAGGCTTGGCAACCCA

Table 2: Primer sequences used for RT-qPCR.

7.2 Results

The mean quality value expected was a Q score of 30 which indicates a 99.9% of accuracy (Fig. 22 and 23).

7.2.1 Pilot study: RNA sequencing analysis

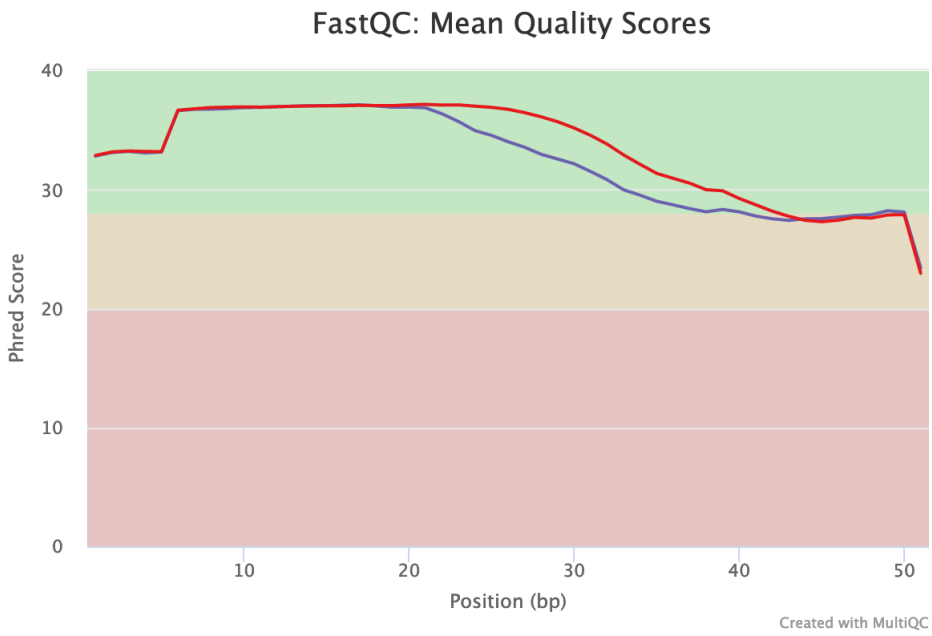

Figure 22: **Sequence Quality Histogram.** The mean quality value across each base position in the read.

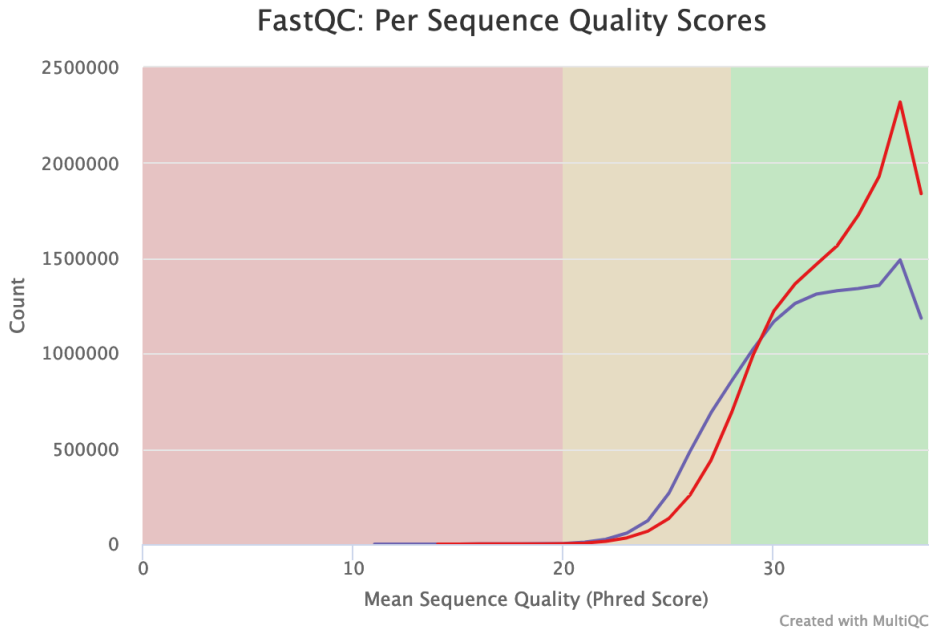

Figure 23: **Per Sequence Quality Scores.** The number of reads with average quality scores.

7.2.2 Proteomic analysis

Most of the proteins identified are listed in the following tables and are classified according to the strain of *C. acnes* in which they were found. Some of the proteins are not fully annotated thus, there are some biological processes, molecular functions and cellular components that are not detailed.

A1 unique proteins

Gene name	Accession	Protein name	GO -Biological process	GO -Cellular component	GO -Molecular function
acpP	D4HDE2	Acyl carrier protein	Fatty acid biosynthesis	Cytoplasm	Acyl carrier activity
argR	A0A2B7J1Q0	Arginine repressor	Arginine biosynthetic process	Cytoplasm	Arginine binding, DNA binding, repressor
argS	D1YE93	Arginine-tRNA ligase	Protein biosynthesis	Cytoplasm	Catalytic activity: Aminoacyl-tRNA synthetase, Ligase
CHT92_00425	A0A2B7IXI0	ABC transporter permease subunit	Transmembrane transport	Plasma membrane	
CHT92_04885	A0A2B7II03	ABC transporter substrate-binding protein	Transmembrane transport	Plasma membrane	
CHT92_05575	A0A2B7JV00	Permease IIC component	Sugar transport	Plasma membrane	Protein-N(PI)-phosphohistidine-sugar phosphotransferase activity
CHT92_07640	A0A3E2DJI4	DUF3040 domain-containing protein		Plasma membrane, integral component of the membrane	
CHT92_10825	A0A3A8VS65	Methionine ABC transporter substrate-binding protein		Plasma membrane	
CHT92_10850	A0A2B7JMV7	PspC domain-containing protein		Plasma membrane	
CHT92_11260	A0A3E2DDL1	Peptide ABC transporter substrate-binding protein	Transmembrane transport	Plasma membrane	
CHT92_12705	A0A2B7JN69	Uncharacterized protein		Plasma membrane, integral component of the membrane	
dacB	A0A533IPY3	D-alanyl-D-alanine carboxypeptidase/D-alanyl-D-alanine-endopeptidase		Plasma membrane, integral component of the membrane	Catalytic activity: carboxypeptidase, hydrolase, protease
dapF	A0A5R8PYG8	Diaminopimelate epimerase	Amino-acid biosynthesis, Lysine biosynthesis	Cytoplasm	Catalytic activity: isomerase
DI580_05850	A0A533IMQ5	Hyaluronate lyase	Carbohydrate metabolic process	Extracellular region	Catalytic activity: lyase; carbohydrate binding
DI580_05850	A0A533IMQ5	Hyaluronate lyase	Pathogenesis, Carbohydrate metabolic process	Extracellular region	Catalytic activity: lyase; carbohydrate binding
dnaA	A0A2B7IZL1	Chromosomal replication initiator protein DnaA	DNA replication initiation, regulation of DNA replication	Cytoplasm	ATP binding, DNA binding
FD514_01075	A0A2B7IG34	FtsQ-type POTRA domain-containing protein	Cell cycle, cell division	Plasma membrane, integral component of the membrane	
FD514_05935	A0A5R8PVD9	Uncharacterized protein		Plasma membrane, integral component of the membrane	
FD514_06410	A0A5R8PUG9	Dihydroorotate dehydrogenase-like protein	Pyrimidine biosynthesis	Cytoplasm	Catalytic activity: oxidoreductase
FD514_07925	A0A5R8PQ47	Cation diffusion facilitator family transporter		Plasma membrane	Cation transmembrane transporter activity
FD514_08135	A0A5R8PQV4	MFS transporter		Plasma membrane	Transmembrane transporter activity
FD514_08250	A0A2B7I5X6	Phosphoesterase	Pathogenesis, Virulence		Catalytic activity: hydrolase
FD518_02880	A0A5R8PWP9	DUF58 domain-containing protein		Plasma membrane, integral component of the membrane	
FD518_03035	A0A5R8PX27	Uncharacterized protein		Plasma membrane, integral component of the membrane	
FD518_03070	A0A2B7J1V7	Cytochrome bc1 complex Rieske iron-sulfur subunit		Plasma membrane	Metal ion binding
FD518_05985	A0A2B7IZW4	APC family permease		Plasma membrane	Transmembrane transporter activity
FD518_06240	A0A2B7IZH7	Uncharacterized protein	GPI anchor biosynthetic process	Plasma membrane	Catalytic activity: Glycosyltransferase, transferase
FD518_07610	A0A2B7JP30	Phosphomannomutase	GDP-mannose biosynthetic process	Cytoplasm	
FD518_10200	A0A2B7INF5	Thrombospondin	Cell adhesion		Calcium ion binding, hydrolase activity
glmS	A0A2B7JMT7	Glutamine--fructose-6-phosphate aminotransferase [isomerizing]	Carbohydrate derivative biosynthetic process	Cytoplasm	Catalytic activity: aminotransferase, transferase

Gene name	Accession	Protein name	GO -Biological process	GO -Cellular component	GO -Molecular function
groL	A0A533IIY4	60 kDa chaperonin	Protein refolding	Cytoplasm	ATPase activity
gyrA	A0A2B7ID62	DNA gyrase subunit A	DNA dependent DNA replication, DNA topological change	Cytoplasm	Catalytic activity: Isomerase, topoisomerase
hemE	Q6AB03	Uroporphyrinogen decarboxylase	Porphyrin biosynthesis	Cytoplasm	Catalytic activity: decarboxylase, lyase
hemL	A0A2B7ICM6	Glutamate-1-semialdehyde 2,1-aminomutase	Protoporphyrinogen IX biosynthetic process	Cytoplasm	Catalytic activity: isomerase
hisF	D4HEQ8	Imidazole glycerol phosphate synthase subunit HisF	Histidine biosynthetic process	Cytoplasm	Catalytic activity: lyase
HMPREF0675_3387	D4HAP6	Uncharacterized protein		Plasma membrane, integral component of the membrane	
HMPREF0675_3781	D4HCN7	Cytochrome bc1 complex cytochrome c subunit	Electron transport, Respiratory chain, Transport	Plasma membrane	Catalytic activity: translocase
HMPREF0675_3781	D4HCN7	Cytochrome bc1 complex cytochrome c subunit	Electron transport, Respiratory chain, Transport	Plasma membrane	Catalytic activity: translocase
HMPREF0675_3798	D4HCQ4	Non-specific serine/threonine protein kinase		Plasma membrane, integral component of the membrane	Catalytic activity: kinase, transferase
HMPREF0675_3846	D4HCV1	Sortase family protein		Plasma membrane, integral component of the membrane	
HMPREF0675_3857	D4HCW2	HtaA domain protein		Plasma membrane, integral component of the membrane	
HMPREF0675_3979	D4HD82	DoxX family protein		Plasma membrane	
HMPREF0675_4553	D4HF32	3-dehydroquinate synthase	Phospholipid biosynthetic process	Cytoplasm	Catalytic activity: oxidoreductase
HMPREF0675_4634	D4HFI0	DsbA-like protein		Plasma membrane, integral component of the membrane	
HMPREF0675_4709	D4H964	Glycosyl hydrolase family 25	Pathogenesis, cell wall macromolecule catabolic process		Lysozyme activity and Catalytic activity: glycosidase, hydrolase
HMPREF0675_4749	D4H9A5	Cell envelope-like function transcriptional attenuator common domain protein	Plasma membrane, integral component of the membrane		
HMPREF0675_4856	D4H9R8	Triacylglycerol lipase	Catalytic activity: hydrolase	Pathogenesis, Lipid catabolic process	
HMPREF0675_5375	D4HBM4	Transporter, small conductance mechanosensitive ion channel MscS family protein	Transmembrane transport	Plasma membrane	
HMPREF1162_1120	F9NWW6	Phosphoenolpyruvate--glycerone phosphotransferase	Glycerol catabolic process	Plasma membrane, integral component of the membrane	Catalytic activity: kinase, transferase
HMPREF9206_0385	D1YEZ5	Mannosyl-glycoprotein endo-beta-N-acetylglucosaminidase	Metabolic process	Cytoplasm	Catalytic activity: glycosidase, hydrolase
HMPREF9206_1920	D1YCI4	Amino acid permease	Amino acid transport, transmembrane transport	Plasma membrane, integral component of the membrane	
HMPREF9206_2337	D1YBB3	Uncharacterized protein		Plasma membrane, integral component of the membrane	
hppA	A0A2B7JMR3	K (+)-insensitive pyrophosphate-energized proton pump	Hydrogen ion transport	Plasma membrane	Catalytic activity: hydrolase translocase
hutI	A0A3E2DFU2	Imidazolonepropionase	Histidine metabolism	Cytoplasm	Catalytic activity: hydrolase
idi	D4HAW5	Isopentenyl-diphosphate Delta-isomerase	Isoprenoid biosynthetic process	Cytoplasm	Catalytic activity: isomerase
lepA	A0A2B7J1Q5	Elongation factor 4	Positive regulation of translation	Plasma membrane	Elongation factor, hydrolase
leuS	Q6A9B8	Leucine-tRNA ligase	Protein biosynthesis	Cytoplasm	Catalytic activity: Aminoacyl-tRNA synthetase, Ligase
luxS	D4HBR0	S-ribosylhomocysteine lyase	Autoinducer synthesis, quorum sensing		Catalytic activity: lyase
metG	D4H9D5	Methionine-tRNA ligase	Protein biosynthesis	Cytoplasm	Catalytic activity: Aminoacyl-tRNA synthetase, ligase

Gene name	Accession	Protein name	GO -Biological process	GO -Cellular component	GO -Molecular function
metK	A0A2B7IH87	S-adenosylmethionine synthase	One-carbon metabolism, S-adenosylmethionine biosynthetic process	Cytoplasm	Catalytic activity: transferase
metN	A0A2B7I5Y0	Methionine import ATP-binding protein MetN	Amino acid transport	Plasma membrane	Catalytic activity: translocase
mfd	D4HC57	Transcription-repair-coupling factor	Regulation of transcription, DNA damage recognition	Cytoplasm	DNA binding, Helicase activity
murE	A0A2B7II35	UDP-N-acetylmuramoyl-L-alanyl-D-glutamate--2,6-diaminopimelate ligase	Cell cycle, cell division	Cytoplasm	Catalytic activity: ligase
nadK	A0A2B7I419	NAD-Kinase	NAD metabolic process, NADP biosynthetic process	Cytoplasm	Catalytic activity: kinase, transferase
ndk	A0A2B7IGB9	Nucleoside diphosphate kinase	Nucleotide metabolism	Cytoplasm	Catalytic activity: kinase, transferase
nhaA	A0A2B7ICU2	Na (+)/H (+) antiporter NhaA	Regulation of pH	Plasma membrane	Antiporter activity: ion and sodium transport.
pfp	D1YCG3	Pyrophosphate-fructose 6-phosphate 1-phosphotransferase	Glycolysis	Cytoplasm	Catalytic activity: kinase, transferase
pgi	A0A2B7IQH6	Glucose-6-phosphate isomerase	Gluconeogenesis, glycolysis	Cytoplasm	Catalytic activity: isomerase
PPA0294	Q6AB14	PTS system sugar-specific EII component	Phosphoenolpyruvate-dependent sugar phosphotransferase system	Plasma membrane	Catalytic activity: kinase, transferase
PPA0467	Q6AAJ7	Putative sugar transporter YfiG	Sugar transport	Plasma membrane	Transmembrane transporter activity
PPA1035	Q6A8X9	Putative lipase		Plasma membrane, integral component of the membrane	Catalytic activity: triglyceride lipase activity
PPA1570	Q6A7F2	Tricorn protease homolog		Cytoplasm	Hydrolase, Protease, Serine protease
PPA1677	Q6A756	Ferrous iron transport protein B		Plasma membrane, integral component of the membrane	Ferrous iron transmembrane transporter activity, GTP binding
PPA2027	Q6A672	Putative two component sensor kinase		Plasma membrane, integral component of the membrane	Catalytic activity: kinase, transferase
PPA2254	Q6A5K6	Amino acid permease	Amino acid transport, transmembrane transport	Plasma membrane, integral component of the membrane	
priA	A0A2B7IHA3	1-(5-phosphoribosyl)-5-[(5-phosphoribosylamino) methylideneamino] imidazole-4-carboxamide isomerase	Amino-acid biosynthesis, Histidine biosynthesis	Cytoplasm	Catalytic activity: isomerase
ptsP	A0A3E2DPZ4	Phosphoenolpyruvate-protein phosphotransferase	Phosphotransferase system, sugar transport, transport	Cytoplasm	Catalytic activity: kinase, transferase
purC	A0A3D8Z377	Multifunctional fusion protein	Purine biosynthesis	Cytoplasm	Catalytic activity: ligase
rbsK	Q6ABP7	Ribokinase	Carbohydrate metabolism	Cytoplasm	Catalytic activity: kinase, transferase
recF	D4HEG2	DNA replication and repair protein RecF	DNA repair, DNA replication, SOS response	Cytoplasm	ATP-binding, single-stranded DNA binding
rimO	Q6A908	Ribosomal protein S12 methylthiotransferase RimO	Peptidyl-L-beta-methylthioaspartic acid biosynthetic process from peptidyl-aspartic acid, tRNA modification	Cytoplasm	Catalytic activity: transferase
rnhA	D1YER5	Ribonuclease H	RNA catabolic process	Cytoplasm	Catalytic activity: endonuclease, hydrolase, nuclease
rsmG	Q6A5B2	Ribosomal RNA small subunit methyltransferase G	rRNA processing	Cytoplasm	Catalytic activity: methyltransferase, transferase
rsmI	A0A2B7ICI1	Ribosomal RNA small subunit methyltransferase I	rRNA processing	Cytoplasm	Catalytic activity: methyltransferase, transferase
secF	A0A2B7J2E2	Protein-export membrane protein SecF	Intracellular protein transmembrane transport	Plasma membrane	P-P-bond-hydrolysis-driven protein transmembrane transporter activity

Gene name	Accession	Protein name	GO -Biological process	GO -Cellular component	GO -Molecular function
ung	D4HC75	Uracil-DNA glycosylase	Base-excision repair	Cytoplasm	Catalytic activity: hydrolase
uvrB	A0A3E2DJD2	UvrABC system protein B	Nucleotide-excision repair, SOS response	Cytoplasm	Excision nuclease
valS	D1YDG1	Valine-tRNA ligase	Protein biosynthesis	Cytoplasm	Catalytic activity: Aminoacyl-tRNA synthetase, Ligase
xseB	A0A533INZ9	Exodeoxyribonuclease 7 small subunit	DNA catabolic process	Cytoplasm	Exonuclease, Hydrolase, nucelase
yvcK	A0A2B7JVP4	Putative gluconeogenesis factor	Regulation of cell shape	Cytoplasm	LPPG:FO 2-phospho-L-lactate transferase activity

Table 3: Proteins identified in A1 EVs.

H1 unique proteins

Gene name	Accession	Protein name	GO -Biological process	GO -Cellular component	GO -Molecular function
argS	D1YE93	Arginine-tRNA ligase	Protein biosynthesis	Cytoplasm	Catalytic activity: Aminoacyl-tRNA synthetase, Ligase
cbiN	A0A2B7IYZ6	Cobalt transport protein CbiN	Cobalamin biosynthetic process	Plasma membrane	Cobalt ion transmembrane transporter activity
CHT92_00705	A0A2B7IXV0	NfeD family protein		Plasma membrane, integral component of the membrane	
CHT92_01965	A0A3E2DPS5	Histidine kinase		Plasma membrane, integral component of the membrane	Kinase and transferase activity
CHT92_02570	A0A3E2DQ40	Two-component sensor histidine kinase		Plasma membrane, integral component of the membrane	Kinase and transferase activity
CHT92_08935	A0A2B7JNS3	Transporter	Potassium ion transport	Plasma membrane, integral component of the membrane	Cation transmembrane transporter activity
CHT92_09525	A0A371N6V9	ABC transporter substrate-binding protein	Transmembrane transport	Plasma membrane	
CHT92_10445	A0A371N5H5	Phosphoheptose isomerase	Carbohydrate metabolic process		Catalytic activity: isomerase
CHT92_10835	A0A2B7I5R4	ABC transporter permease	Transmembrane transport	Plasma membrane	
ctaD	A0A5R8PZ71	Cytochrome c oxidase subunit 1	Electron transport, Respiratory chain, Transport		Catalytic activity: oxidoreductase
DI580_03525	A0A533IMY9	Threonine/serine exporter family protein		Plasma membrane, integral component of the membrane	
FD514_01875	A0A5R8PYL0	Sensor histidine kinase		Plasma membrane, integral component of the membrane	Kinase and transferase activity
FD514_08195	A0A5R8PQG9	HlyC/CorC family transporter		Plasma membrane, integral component of the membrane	Flavin adenine dinucleotide binding
FD514_10805	A0A371N4W3	Glycoside hydrolase family 13 protein	Carbohydrate metabolic process		Catalytic activity: hydrolase
FD518_04795	A0A2B7ICE8	Sugar ABC transporter permease	Transmembrane transport	Plasma membrane	
FD518_06560	A0A2B7JSI7	MMPL family transporter		Plasma membrane	
PPA2063	Q6A637	Peptide ABC transporter substrate-binding protein	Transmembrane transport	Plasma membrane	
PPA2066	Q6A634	ATP-binding protein of dipeptide ABC transporter	Peptide transport		ATPase activity, ATP binding
PPA2346	Q6A5A8	Alanine racemase	Alanine metabolic process		Alanine racemase activity
purA	Q6A6A3	Adenylosuccinate synthetase	Purine biosynthesis	Cytoplasm	Catalytic activity: ligase
rpsR	A0A533IPV3	30S ribosomal protein S18	Translation	Ribosome	rRNA binding, structural constituent of ribosome
valS	D1YDG1	Valine-tRNA ligase	Protein biosynthesis	Cytoplasm	Catalytic activity: Aminoacyl-tRNA synthetase, Ligase

Gene name	Accession	Protein name	GO -Biological process	GO -Cellular component	GO -Molecular function
ndk	D1Y9W2	Nucleoside diphosphate kinase	Nucleotide metabolism	Cytoplasm	Catalytic activity: kinase, transferase
nuoG	D1YFB4	NADH-quinone oxidoreductase	ATP synthesis coupled electron transport	Plasma membrane	Catalytic activity: oxidoreductase, translocase
nuoK	A0A533ITF7	NADH-quinone oxidoreductase subunit K	ATP synthesis coupled electron transport	Plasma membrane	Oxidoreductase, Translocase: NADH dehydrogenase (quinone) activity, quinone binding
pgsA	A0A533IRH7	CDP-diacylglycerol-glycerol-3-phosphate 3-phosphatidyltransferase	Phospholipid biosynthetic process	Plasma membrane, integral component of the membrane	CDP-diacylglycerol-glycerol-3-phosphate 3-phosphatidyltransferase activity
PPA0540	Q6AAC3	Conserved protein		Plasma membrane, integral component of the membrane	Hydrolase, Metalloprotease, Protease
PPA0717	Q6A9U2	Conserved protein, putative regulatory protein		Plasma membrane, integral component of the membrane	
PPA1091	Q6A8S8	Hypothetical membrane associated protein		Plasma membrane, integral component of the membrane	
PPA1142	Q6A8M6	PTS system, sucrose-specific IIBC component	Phosphoenolpyruvate-dependent sugar phosphotransferase system	Plasma membrane	Kinase activity
PPA1329	Q6A837	Glutamate dehydrogenase	Glutamate catabolic process to 2-oxoglutarate		Catalytic activity: oxidoreductase
PPA1569	Q6A7F3	Conserved protein (Sialidase-like protein)			Carbohydrate binding, Glycopeptide alpha-N-acetylgalactosaminidase activity
PPA1570	Q6A7F2	Tricorn protease homolog		Cytoplasm	Hydrolase, Protease, Serine protease
PPA2012	Q6A686	Uncharacterized protein		Plasma membrane, integral component of the membrane	
PPA2063	Q6A637	Peptide ABC transporter substrate-binding protein	Transmembrane transport	Plasma membrane	
folE	D1Y9P6	GTP cyclohydrolase 1	One-carbon metabolism		Catalytic activity: hydrolase
gcvP	A0A6B7F554	Glycine dehydrogenase (decarboxylating)	Glycine decarboxylation via glycine cleavage system		Catalytic activity: oxidoreductase
glmS	Q6A6T9	Glutamine-fructose-6-phosphate aminotransferase [isomerizing]	Carbohydrate derivative biosynthetic process, carbohydrate metabolic process, glutamine metabolic process	Cytoplasm	Catalytic activity: aminotransferase, transferase
gyrB	A0A2B7INC6	DNA gyrase subunit B	DNA-dependent DNA replication, DNA topological change	Cytoplasm	Catalytic activity: Isomerase, topoisomerase
HMPREF0675_3728	D4HCI3	Carbon starvation protein CstA	Transport: cellular response to starvation	Plasma membrane	
HMPREF0675_3781	D4HCN7	Cytochrome bc1 complex cytochrome c subunit	Electron transport, Respiratory chain, Transport	Plasma membrane	Catalytic activity: translocase
HMPREF0675_5272	D4HBC2	Transporter, CPA2 family		Plasma membrane, integral component of the membrane	Solute: proton antiporter activity
HMPREF9206_0241	D1YEK3	Uncharacterized protein		Plasma membrane, integral component of the membrane	
HMPREF9206_0856	D1YD98	6-phosphofructokinase	Glycolysis	Cytoplasm	Catalytic activity: kinase, transferase
HMPREF9206_2141	D1Y9V9	S1 RNA binding domain protein	RNA processing		Hydrolase, RNA-binding
hutH	Q6A5T7	Histidine ammonia-lyase	Histidine metabolism	Cytoplasm	Catalytic activity: lyase
leuS	Q6A9B8	Leucine-tRNA ligase	Protein biosynthesis	Cytoplasm	Catalytic activity: Aminoacyl-tRNA synthetase, Ligase
metG	Q6A707	Methionine-tRNA ligase	Protein biosynthesis	Cytoplasm	Catalytic activity: Aminoacyl-tRNA synthetase, Ligase
mraW	D4HCS4	Ribosomal RNA small subunit methyltransferase H	rRNA processing	Cytoplasm	Catalytic activity: methyltransferase, transferase
nadE	A0A2B7I9S8	Glutamine-dependent NAD (+) synthetase	NAD biosynthetic process	Cytoplasm	Catalytic activity: ligase

Table 4: Proteins identified in H1 EVs.

KPA unique proteins

Gene name	Accession	Protein name	GO -Biological process	GO -Cellular component	GO -Molecular function
arcA	D1YBM8	Arginine deiminase	Arginine metabolism	Cytoplasm	Catalytic activity: hydrolase
argF	D1YBM7	Ornithine carbamoyltransferase		Cytoplasm	Transferase: amino acid binding
CHT92_07205	A0A2B7IQB1	Uncharacterized protein		Plasma membrane, integral component of the membrane	
CHT92_08615	A0A2B7JWN3	DUF4307 domain-containing protein		Plasma membrane, integral component of the membrane	
cysK	D1YD21	Cysteine synthase	Cysteine biosynthesis		Catalytic activity: transferase
FD514_10465	A0A5R8PSU7	Lipopolysaccharide biosynthesis protein		Plasma membrane, integral component of the membrane	
HMPREF9206_0041	D1YDP4	Uncharacterized protein		Plasma membrane, integral component of the membrane	
HMPREF9206_0420	D1YF30	ABC transporter, substrate-binding protein, family 5	Transmembrane transport	Plasma membrane	
HMPREF9206_0602	D1YE01	Fructose-bisphosphate aldolase class I	Glycolytic process		Catalytic activity: lyase
HMPREF9206_0861	D1YFG9	ErfK/YbiS/YcfS/YnhG	Peptidoglycan biosynthetic process		Catalytic activity: acyltransferase, transferase
HMPREF9206_1052	D1Y918	Catalase	Hydrogen peroxide catabolic process, response to oxidative stress		Catalytic activity: oxidoreductase, peroxidase
HMPREF9206_1092	D1Y957	Uncharacterized protein		Plasma membrane, integral component of the membrane	
HMPREF9206_1884	D1YCF3	PPIase cyclophilin-type domain-containing protein			Catalytic activity: isomerase
HMPREF9206_2198	D1YA15	Antigen 84	Cell cycle, cell division	Cytoplasm	
HMPREF9206_2295	D1YAN0	Phosphotransferase system, EIIB	Phosphotransferase system		Catalytic activity: transferase
kup	Q6A5S0	Probable potassium transport system protein kup	Ion transport, Potassium transport, Transport	Plasma membrane	Potassium ion transmembrane transporter activity
pdxS	D1YD19	Pyridoxal 5'-phosphate synthase subunit PdxS	Pyridoxal phosphate biosynthetic process		Catalytic activity: lyase
pgk	D1Y9W8	Phosphoglycerate kinase	Glycolytic process	Cytoplasm	Phosphoglycerate kinase activity, ATP binding
PPA0185	Q6ABC3	Cell division protein FtsI	Cell cycle, cell division		Penicillin binding
PPA0990	Q6A923	Endo-beta-N-acetylglucosaminidase H	Carbohydrate metabolic process	Extracellular region	Mannosyl-glycoprotein endo-beta-N-acetylglucosaminidase activity
PPA1345	Q6A817	DUF1707 domain-containing protein		Plasma membrane, integral component of the membrane	
PPA1579	Q6A7E3	Peptidase (Peptidase family S51)			Hydrolase, Protease, Serine protease
PPA1738	Q6A6Z7	Isocitrate dehydrogenase [NADP]	Glyoxylate bypass, Tricarboxylic acid cycle		Catalytic activity: oxidoreductase
PPA1948	Q6A6E7	Conserved protein with phosphatase domain of diacylglycerol kinase	Glycerol metabolic process		Glycerone kinase activity
pstS	D1YA84	Phosphate-binding protein PstS	Phosphate ion transmembrane transport	Plasma membrane	Phosphate ion binding
sufD	D1YDE1	FeS assembly protein SufD	Iron-sulfur cluster assembly		
sufS	D1YDD8	Cysteine desulfurase	Cysteine metabolic process		Cysteine desulfurase activity, pyridoxal phosphate binding

Table 5: Proteins identified in KPA EVs.